mm-Wave Radar-Based Indoor and Outdoor Parking Monitoring and Management

Thesis by

Yingquan Li

In Partial Fulfillment of the Requirements

For the Degree of

Masters of Science

King Abdullah University of Science and Technology

Thuwal, Kingdom of Saudi Arabia

April,2022

EXAMINATION COMMITTEE PAGE

The thesis of Yingquan Li is approved by the examination committee

Committee Chairperson: Prof. Mohamed-Slim Alouini
Committee Members: Prof. Basem Shihada, Prof. Atif Shamim

©April,2022

Yingquan Li

All Rights Reserved

ABSTRACT

mm-Wave Radar-Based Indoor and Outdoor Parking Monitoring and Management

Yingquan Li

Multistory parking can accommodate a maximum number of vehicles in a limited space. However, in multistory and outdoor busy parking, it becomes challenging for drivers to find free parking slots, and they have to search in different parking lanes and floors. This results in the wastage of fuel and time and contaminates the atmosphere. To address this issue, the state-of-the-art solution exploits an optical sensor to detect if a car is present in the parking slot or not. The solution requires an optical sensor for each parking slot, which makes the optical sensor solution expensive and complex. Moreover, such a solution fails in harsh weather conditions in outdoor parking. A low-cost mm-wave radar-based solution is proposed to detect multiple cars using only one radar and pass the corresponding information to the developed computer/mobile app. Using the app, users can view the free parking slots in advance. Our proposed solution also provides free parking slot information at the parking entrance. A driver can select one from the available ones and park his car there. In the next version, people will be able to book the parking slots from the available ones. To detect the presence of vehicle in multiple parking slots, our proposed system uses Infineon's Postion2Go module, which is one transmit and two receive antenna frequency-modulated continuous-wave (FMCW) radar. We develop a parking model using stationary objects, clutter, and vehicles in the parking. The vehicle detection algorithm is based on background subtraction and updation. First, the background is subtracted from each received snapshot to prominent the parking slot where the latest

activity has been done. Then, once the activity is stable (the vehicle is fully parked or left), the background is updated. The algorithm also uses constant-false-alarm-rate (CFAR) for adaptive detection of vehicles and thresholds to detect different activities. The method of monitoring outdoor parking is simple, while the indoor parking is more challenging. Demonstrated results show the effectiveness of the proposed system.

ACKNOWLEDGEMENTS

I would like to express my appreciation to my supervisor: Prof. Mohamed-Slim Alouini. Thank you for agreeing to my application for CTL and his extremely helpful guidance in both courses and research. I would also like to thank Prof. Sajid Ahmed for his detailed support and help. Thank you for all the important meetings in encouraging me to think, execute and implement from multiple perspectives.

I would like to thank my committee members: Prof. Basem Shihada and Prof. Atif Shamim for their time and discussion. They gave me positive feedback and significant comments to guide me to improve my work.

Finally, I would like to thank my parents and all my friends. Thank them for their deep love and all the unconditional support. This spiritual strength is an important backing for me to complete my studies

TABLE OF CONTENTS

Examination Committee Page **2**

Copyright **3**

Abstract **4**

Acknowledgements **6**

Table of Contents **7**

List of Figures **9**

List of Tables **12**

1 Introduction **13**
1.1 Related Work 14
1.2 Organization 15

2 FMCW Radar Signal Model and CFAR principle **16**
2.1 Introduction 16
2.2 Signal Model 18
2.3 Range Based Outdoor Parking Monitoring 22
2.4 CFAR Algorithm 25
2.5 Preliminary results 32

3 Background Subtraction-based Algorithm **35**
3.1 Introduction 35
3.2 Solution for sidelobe leakage and background noise 36
3.3 The steps of background subtraction-based algorithm 37
3.3.1 Unblocked Radar Field-of-View 38

3.3.2 Blocked Radar Field of View 41
3.3.3 Cars Block Radar Field of View and Multiple Cars Enter and Exit . . 45
3.4 System Performance Analysis 50
3.4.1 Monitoring System Capacity 50
3.4.2 Radar Height 50
3.5 Conclusion 53

4 Experiment Results **56**

5 Robust target estimation algorithm **62**
5.1 Targets' Estimation with Forward Samples 62
5.2 Target's Estimation with Forward-Backward Samples 64

6 Future work **72**

7 Conclusion **74**

References **76**

LIST OF FIGURES

2.1 An example of a chirp in time and frequency domain, respectively. . . 19
2.2 Correct detection is result from two cases: H_0 is true and D_0 is true, or H_1 is true and D_1 is true. False dismissal means H_1 is true and D_0 is true. False alarm means H_0 is true and D_1 is true. CFAR algorithm is proposed to avoid false alarm. 26
2.3 Except guard cells, The mean square amplitude of a certain number of adjacent sampling points is calculated. They are called training cells. In our practice, there are guard cells and training cells on both sides. The level of the cell to be detected will be compared with the mean square amplitude of training cells to determine whether there is really a target. 29
2.4 There is one car in 8.75m which is also the location of the third parking slot. And that corresponds to the peak in the figure. However, there are also other small peaks and impulses. They result from obstacles such as pillars and pipes and sidelobe leakage. 33
2.5 The optical reference of Fig. 2.4 33
2.6 The red line is the amplitude spectrum of Fig. 2.4 and the green line is the corresponding thresholds given by CFAR. Many peaks are considered as obstacles because of their low level. 34

3.1 The effect of Hamming windowing function. The envelope reduced clearly comparing with the original signal 36
3.2 The Signal power varies widely from different sources. The noise power is very weak and can be ignored. The reflection of obstacles such as pillars and pipes are closer than a car if the car is parked far away. . 37
3.3 Proposed algorithm flow chart when a car does not block radar FoV, where PS stands for parking slot and the values of $\eta(i_1)$, $\eta(i_2)$ inversely proportional to the range. 40

3.4 Entering or exiting car does not block the radar FoV and one car moves at a time. In such scenario the BS subtraction from received signal generates only one peak. 42
3.5 Proposed algorithm flowchart when entering or exiting car blocks the radar FoV but one car moves at a time. 43
3.6 Entering or exiting car blocks the radar FoV and one car moves at a time. In such scenario the BS subtraction from received signal can generate more than one peak. 45
3.7 Generalized proposed algorithm flowchart for anti-blocking and multiple car movement detection, where ρ is a threshold value. 47
3.8 Entering or exiting cars block the radar FoV and more than one car can move at a time. In such scenario, the BS subtraction from received signal can generate more than one peak. 48
3.9 A radar is installed at height h, parking slots $A, B, \ldots, E$ are in its field of view. 51
3.10 Because the range difference is increasing with N increasing, FMCW radar has infinite capacity 52
3.11 The middle smaller car is blocked by the bigger car parked in the 1st parking slot. But the car in 3rd parking slot is in the radar FoV. . . . 53
3.12 Increasing the radar height can increase the radar FoV. 54
3.13 Masking influence simplification figure 54

4.1 Indoor parking scene from the radar height in the radar boresight direction. 57
4.2 Measurement layout of the parking lot. 57
4.3 All parking slots are free. 59
4.4 First parking slot is occupied by a golden SUV. 59
4.5 First and 2nd parking slots are respectively occupied by white sedan and golden SUV. 59
4.6 Second and 3rd parking slots are respectively occupied by white sedan and golden SUV. 60
4.7 Third parking slot is occupied by white sedan. 60
4.8 Eight parking slot is occupied by white sedan. 61
4.9 Three cars are parked from the 2nd to the 4th parking slots. Two sedans are in front of the SUV. 61

4.10 Three cars are parked from the 2nd to the 4th parking slots. The SUV is in front of two sedans. But the blockage effect has no influence. . . 61

5.1 Beat frequency estimation using Forward and Forward-Backward sample vector techniques, where $N = 128$ and $M = 10$. 66
5.2 Beat frequency estimation using Forward and Forward-Backward sample vector techniques, where $N = 128$ and $M = 20$. 66
5.3 Target estimation using LR with Forward and Forward-Backward sample vector techniques, where $N = 128$ and $M = 10$. 71
5.4 Target estimation using LR with Forward and Forward-Backward sample vector techniques, where $N = 128$ and $M = 20$. 71

6.1 The flow of parking occupancy data from Position2Go module to Mobile and web applications. 73

LIST OF TABLES

2.1 Parameters in recording raw data. FFT means Fast Fourier Transform. 32

3.1 When a vehicle enters, leaves and remains at rest, the spectral sampling point has a different magnitude relationship to the threshold. By using CFAR for B, Z, and X respectively, the motion of the vehicle can be determined. 46

Chapter 1

Introduction

A few years ago, a simple big yard was more than enough to park cars. Nowadays, parking lots have become so sophisticated, and their only aim is to hold the maximum number of cars. Since the manufacturing cost of cars is dropping day by day, the number of cars is increasing in the cities. For instance, in 20 years from 1985 to 2005, car ownership in China has increased nearly tenfold [1][2]. As a consequence, parking lots are getting packed. Multistory parking lots are available to stack one car on top of the other to cope with parking problems. In big parking lots, finding a free parking slot is another challenge. Sometimes, finding a free parking spot requires a lot of time, which is a wastage of time and money. Moreover, it increases environmental pollution [3]. We propose a new mm-wave FMCW radar-based indoor and outdoor parking monitoring and management system to solve the above challenges. Outdoor environment is easier and can be solved by simply increasing the height of the radar. However, Indoor environment has strict limitation on the height of the radar. We most focus on the indoor parking lot and propose a background recording-based technique. Our proposed system allocates memory for each parking slot and maps each parking slot to a dedicated memory location. Whenever a car enters or leaves the parking slot, the corresponding memory location is updated with 1 or 0, where 1 and 0 respectively represent the parking slot is occupied or free. The Infineon Position2Go module is used to realize the system. The module has an mm-wave radar transceiver of one transmit and two receive antennas, a central processing unit, and memory.

1.1 Related Work

Several radar-based techniques are available in the literature to find free parking slots. These techniques can be classified into two categories. In the first one, radar is mounted on the car, while in the second one, radar is mounted in the parking lot. For example, in [4], four 24GHz radar sensors were mounted on a moving car to find the free parking slots. In this algorithm, a car travels between parked cars, and a mounted radar module on the car transmits and receives the data. The drawback of this scheme is offline processing, which is performed after covering some distance. As a result, the detected free parking slots may have been occupied when the driver returned to park the car. Moreover, the accuracy of the scheme is also poor. Similar work has been done with four 79 GHz radar sensors in [5]. This algorithm also has shortcomings in robustness. The main drawbacks of the radar installed on the moving vehicle are: 1) The range of radar becomes very low due to the low height of installed radar on the car, and it can search only nearby regions. 2) Each car requires modification to install a parking lot monitoring system that significantly increases a car's cost.

Therefore, the better idea is to make intelligent car parking [6]. In intelligent car parking, we can use optical or radar sensors to find free parking slots [7]. This information can be available at the parking entrance to save drivers time to find the free parking slot and money in fuel consumption. The more smart way can be to provide a particular free parking slot to each entrant car and make it obligatory for drivers to park in the given parking slot. Unfortunately, there is no work in this direction. As far as the authors know, no parking lot assigns a free parking slot to a vehicle entering the parking lot. The state-of-the-art car parking lot, such as at the Jeddah International Airport, uses optical sensors to know how many parking slots are available. When parking becomes full, the parking system stops the further entry of vehicles. The optical sensor-based parking lots require sensors and wires for

each parking slot [8]. Therefore, they are costly. Moreover, such parking does not provide the free parking slot information to the driver at the entrance, and drivers have to struggle to find the available parking slots. Radars are becoming popular in commercial applications. If placed at a height location, one radar can monitor a number of parking slots. We can develop algorithms to know if individual parking slots under the field of view of radar are free or occupied. In [9], a radar-based complex parking lot monitoring system is developed, which uses multiple transmit and receive antennas and convolutional-neural-network (CNN). This proposed system has few drawbacks. The first one is that the authors have discussed its use only in outdoor parking lot monitoring. Nowadays, most parking lots are indoor multistory, where a car can block the radar field-of-view to see other cars. The radar field-of-view blocking is not accounted for in this algorithm. In an outdoor environment, the radar field-of-view can be increased by increasing the radar height. However, in an indoor parking lot, we cannot increase radar height after some limit. Therefore, the proposed algorithm in [9] is not applicable for indoor parking lots. The second drawback of this algorithm is that it uses a neural network that can take time to train in advance. The third drawback is that it requires several transmit and receive antennas and bulky package, increasing complexity and cost.

1.2 Organization

The remainder of the thesis is organized as follows. In the next chapter, the signal model of the proposed system is described in Chapter. 2. Chapter. 3 explains our algorithm which is suitable for both outdoor and indoor parking. Demo results are shown in Chapter. 4. Chapter. 5 explains a robust target estimation algorithm which will help us enhance our system and Chapter. 6 shows our potential future work.

Chapter 2

FMCW Radar Signal Model and CFAR principle

2.1 Introduction

Radar has been used in military and civilian applications for decades. The military began using radar to detect objects more than 70 years ago during World War II [10]. Nowadays, Many types of radar are kept using in military field, such as infrared radar and microwave radar [11–14]. Radar detection and stealth as eternal antagonists have attracted the attention of countless military enthusiasts [15–18]. The application of radar in civil field should be more extensive and comprehensive. Radar can be found in applications such as detection, imaging and autonomous driving [19–23]. FMCW radar has the advantages of small size and low power, suitable for detection of multiple targets [24, 25]. So we chose FMCW radar to monitor the parking lot.

Statistical detection theory is a mathematical theory which uses the statistical characteristics of signal and noise to establish the best decision [26, 27]. Hypothesis testing is an important tool for statistical judgment. Signal detection is equivalent to hypothesis testing in mathematical statistics [28, 29]. A hypothesis is a test of the possible conditions or states of an object. For radar or sonar detection, two hypotheses can be selected, that is, the presence or absence of the target.

Due to the existence of noise and the limitation of sample number or sample length, judgment errors are inevitable in the detection process. The problem is how to minimize these errors as much as possible, which is the optimization of the detection system. Errors are generally divided into two kinds, one is missed, the other is false

alarm. In different work situations, the consequences caused by these two kinds of errors are not the same, so different levels of attention may be paid to different errors, which introduces the problem of the best criterion. Under different criteria, there are different decision rules (such as different threshold of decision), which makes the detection system have different false alarm errors and misallocation of missing report. Such criteria include minimum average risk criterion (also known as Bayes criterion), minimax criterion (also known as safety average risk criterion) and Neyman-Pearson criterion (also known as maximum detection probability criterion) [30–32].

Constant False Alarm Rate (CFAR) detection is a technology that radar system can determine the existence of target signal by discriminating the output signal and noise of receiver under the condition of Constant False Alarm probability. In our scenario, the received signal isn't constant for the varying location of cars. The power of the car may be weaker than some obstacles such as pillars in the parking lots. Meanwhile, blockage effect exists between cars. Big SUV may block small sedans so it becomes difficult finding the corresponding peak in the spectrum. So we need CFAR to help us determine adaptive thresholds.

In this chapter, we focus on mathematical expressions of FMCW radar signal and CFAR detection. Sec. 2.2 describes FMCW radar signal model and shows how FMCW radar measures the location information of targets. Sec. 2.3 describes how we can utilize FMCW radar signal to monitor a huge, empty and ideal parking lot. Sec. 2.4 shows the steps of CFAR using adjacent sampling points. Sec. 2.5 shows a numerical result of CFAR and another result gotten from our experiment site. We managed to measure the range of two targets and avoided false alaram by using both FMCW radar and CFAR algorithm.

2.2 Signal Model

An FMCW radar transmits multiple continuous wave signals in a frame and each signal is called a "chirp". we assume a chirp is composed with multiple sinusoidal waves and its frequency increases linearly with time. Fig. 2.1 shows a chirp in time and frequency domain, respectively. The chirp duration time is 20s and the bandwidth of the chirp is 2Hz. The complex time-domain expression of the chirp signal can be written as

$$x(t) = e^{j2\pi\left(f_c t + \frac{S}{2}t^2\right)}, \quad 0 \leq t \leq T. \tag{2.1}$$

where f_c is the starting frequency, T is the chirp period, and $S = \frac{B}{T}$ is the frequency sweep rate, while B is the chirp's bandwidth. The phase of the chirp signal can be written as

$$\Phi(t) = 2\pi\left(f_c t + \frac{S}{2}t^2\right).$$

The instantaneous frequency of the chirp signal can be found by differentiating its phase with respect to time as

$$f(t) = \frac{1}{2\pi}\frac{d\Phi(t)}{dt} = f_c + St.$$

It can be seen that frequency increases linearly from f_c to $f_c + B$. If there are N_t targets in the given scenario at different ranges, the received signal after the reflection from these targets can be written as

$$y(t) \quad = \quad \sum_{p=1}^{N_t} e^{j2\pi[(f_c+f_d)+\frac{St}{2}](t-\tau_p)} + w(t). \tag{2.2}$$

where $\tau_p = \frac{2R_o^p}{c}$ and $w(t)$ is the white Gaussian noise, while R_o^p represent the distance of pth target from the radar at the start of chirp and c is the velocity of electromagnetic wave. Assume, the velocity of pth target is v_p, the range of the target at time t can

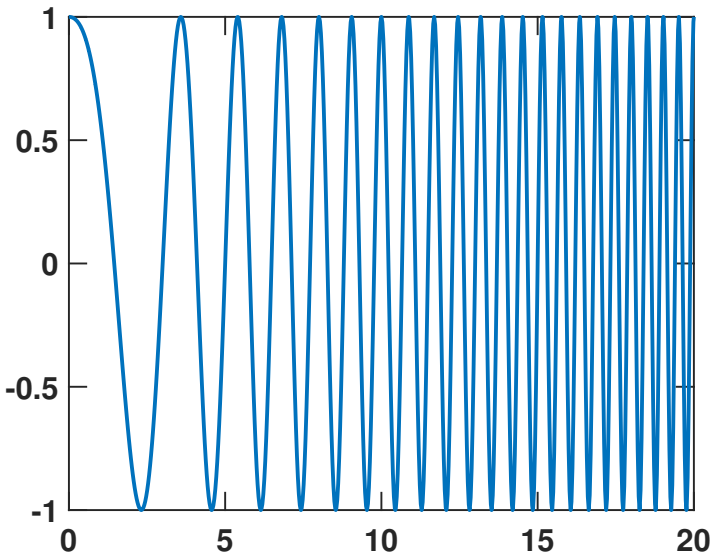

(a) A chirp in time domain

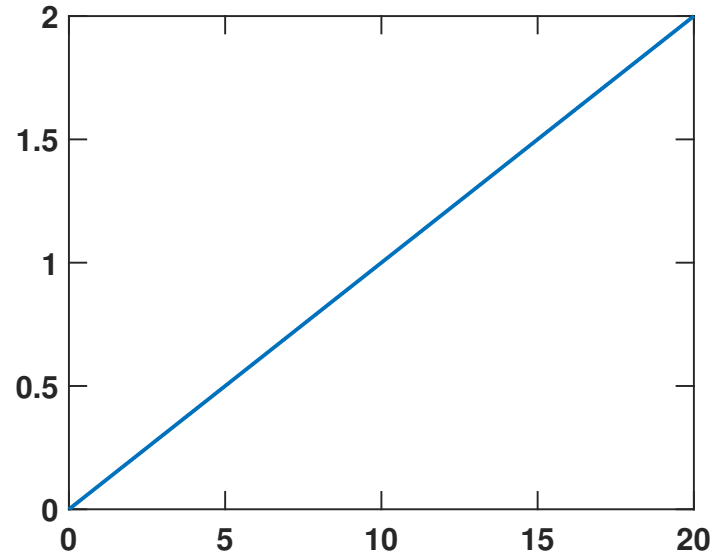

(b) A chirp in frequency domain

Figure 2.1: An example of a chirp in time and frequency domain, respectively.

be written as

$$R_p(t) = R_o^p + v_p t. \tag{2.3}$$

If the duration of the chirp is in micro-seconds and the relative velocity of the target is small ($\leq 2m/s$), for the whole duration of chirp signal, we can write

$$R_p(t) = R_o^p.$$

Demodulating the received signal with the transmitted signal, we can write

$$\begin{aligned} z(t) &= y(t) \times e^{-j2\pi\left(f_c t + \frac{S}{2}t^2\right)}, \\ &= \sum_{p=1}^{N_t} e^{-j2\pi f_c \tau_p \left(1 - \frac{S\tau_p}{2f_c}\right)} e^{-j2\pi S\tau_p t} + \tilde{w}(t), \end{aligned} \tag{2.4}$$

where $\tilde{w}(t) = w(t)e^{-j2\pi\left(f_c t + \frac{S}{2}t^2\right)}$. For practical scenarios $\frac{S\tau_p}{2f_c} \ll 1$, therefore (2.4) can be written as

$$z(t) = \sum_{p=1}^{N_t} e^{-j\frac{4\pi R_o^p}{\lambda}} e^{-j2\pi S\tau_p t} + \tilde{w}(t), \tag{2.5}$$

In (2.5), it can be noticed that inside the summation sign, there are two terms. The first term is constant, while the second term is a complex sinusoidal signal. Therefore, the received signal is a combination of N_t complex sinusoidal signals, and the corresponding frequencies can be found by taking the Fourier transform of (2.5) as

$$Z(f) = \sum_{p=1}^{N_t} e^{j2\pi\left(-f_c\tau_p + \frac{S\tau_p^2}{2}\right)} \int e^{-j2\pi S\tau_p t} e^{-j2\pi f t} dt + \tilde{W}(f). \tag{2.6}$$

The Fourier transform of this signal yields N_t peaks corresponding to different targets given by

$$\begin{aligned} f_p &= S\tau_p, \quad p = 1, 2, \ldots, N_t \\ &= \frac{2BR_o^p}{cT}. \end{aligned} \tag{2.7}$$

Ones frequency corresponding to pth target is estimated, its range can be estimated using (2.7) as

$$R_o^p = \frac{cf_pT}{2B}. \tag{2.8}$$

It should be noted that to sample any frequency f_p, according to Nyquest criterion, $f_p \geq \frac{F_s}{2}$, where F_s is the sampling frequency. Using this fact, the maximum range can be calculated as

$$R_{o\max}^p = \frac{cF_sT}{4B}. \tag{2.9}$$

Therefore, the range of the target can be increased by increasing the pulse width or sampling time or by decreasing the signal's bandwidth. Similarly, to resolve two closely targets, the minimum difference between two adjacent frequencies corresponding to two different targets

$$\Delta f = \frac{1}{T}. \tag{2.10}$$

Using (2.10), the minimum distance between tow target to resolve can be calculated as

$$\begin{aligned} \Delta R &= R_o^{p+1} - R_o^p, \\ &= \frac{cf_{p+1}T}{2B} - \frac{cf_pT}{2B}, \\ &= \frac{c}{2B}. \end{aligned} \tag{2.11}$$

In (2.11), we noticed that in contrast to frequency resolution, the range resolution depends only on the bandwidth of the signal. The following section will exploit the above-derived results to find if parking slots are available or occupied.

2.3 Range Based Outdoor Parking Monitoring

Consider an ideal parking lot scenario. The parking lot is so empty that there are no targets except cars. Besides, the parking lot is huge enough to eliminate multiple path interference. As mentioned in the previous section, where N_t cars are park in a row. To find the presence of cars in different parking slots, we find the range of each car using an FMCW radar. If the radar has one transmit and M receive antennas, we can write the received signal, in the discrete form, at the mth antenna as

$$y_m(n) = \sum_{p=1}^{N_t} e^{jm\pi \sin(\theta_p)} e^{-j\frac{4\pi R_o^p}{\lambda}} e^{j2\pi\left(\frac{B\tau_{op}}{T}\right)n} + w_m(n), \tag{2.12}$$

where $m = 1, 2, \ldots, M$, θ_p is the angular location of pth vehicle and the distance between two adjacent antennas is considered $\lambda/2$. The antennas are arranged in such a way that when the car is parked in the middle of the parking slot, it is in the boresight direction of the antenna array. Taking the discrete-Fourier-transform

(DFT) of (2.12) yields

$$Y_m(k) = \sum_{p=1}^{N_t} e^{jm\pi \sin(\theta_p)} e^{-j\frac{4\pi R_o^p}{\lambda}} \alpha(p,k) + W_m(k), \tag{2.13}$$

where $\alpha(p,k) = \left(\sum_{n=0}^{N-1} e^{j2\pi \left(\frac{B\tau_{op}}{T}\right) n} e^{-j2\pi \frac{kn}{N}} \right)$ and N is the length of DFT points. It should be noted that whenever $\frac{B\tau_{op}}{T} \approx k/N$, there will be a peak that can be used to find the range of the vehicle. If the sampling frequency is F_s, the kth index frequency will correspond to the range of

$$R_{op} = \frac{F_s cT}{2NB} k. \tag{2.14}$$

Since (2.13) is a combination of multiple non-linear terms of $\sin(\theta_p)$, it is challenging to estimate angular location of multiple vehicles. However, we also know that if $\frac{B\tau_{op}}{T} k/N$, $\alpha(p,k) \approx 0$, this can simplify the problem to estimate the angular location of multiple vehicles. Using this fact, the contribution of terms other than the target at kth index location can be ignored, and the sample corresponding to the vehicle location can be written as

$$Y_m(k_p) = e^{jm\pi \sin(\theta_p)} e^{-j\frac{4\pi R_o^p}{\lambda}} \alpha(p,k_p) + W_m(k_p), \tag{2.15}$$

where $k_p = 1, 2, \ldots, N_t$ is the index of location at which target is present. If we have M receive antennas, the above equation for the target at k_p index location in vector form can be written as

$$\mathbf{Y}_{k_p} = e^{-j\frac{4\pi R_o^p}{\lambda}} \alpha(p,k_p) \begin{bmatrix} 1 \\ e^{j\pi \sin(\theta_p)} \\ \vdots \\ e^{j(M-1)\pi \sin(\theta_p)} \end{bmatrix} + \mathbf{W}_{k_p}. \tag{2.16}$$

By multiplying $\mathbf{Y}_{k_p}$ with a beamformer search vector $\mathbf{w} = \begin{bmatrix} 1 & -e^{j\pi\sin(\phi)} & \dots & -e^{j(M-1)\pi\sin(\phi)} \end{bmatrix}^T$ and varying ϕ the location of the vehicle corresponding to this peak can be easily found as

$$\theta_p = \max_{\phi} \left| \mathbf{w}^H \mathbf{Y}_{k_p} \right|.$$

If we have only two antennas, a closed form solution to estimate the location of vehicle can also be found. In the case of two antennas, using (2.15), the receive signals can be written as

$$\begin{aligned} Y_1(k_p) &= e^{-j\frac{4\pi R_o^p}{\lambda}} \alpha(p, k_p) + W_1(k_p), \\ Y_2(k_p) &= e^{j\pi\sin(\theta_p)} e^{-j\frac{4\pi R_o^p}{\lambda}} \alpha(p, k_p) + W_2(k_p), \end{aligned} \tag{2.17}$$

where we have assumed the reference phase is equal to zero. The phase-difference, ϕ_{12}, between $Y_1(k_p)$ and $Y_2(k_p)$ can be found as

$$\begin{aligned} \phi_{12} &= \underline{/\mathbb{E}\{Y_1(k_p)\}\mathbb{E}\{Y_2^*(k_p)\}}, \\ &= \arctan\left(\frac{x_1x_2 + y_1y_2}{x_2y_1 - x_1y_2}\right), \\ &= \pi\sin(\theta_p), \end{aligned} \tag{2.18}$$

where x_p and y_p are used to represent the real and imaginary parts of $Y_p(k_p)$, while, expectation minimises the contribution of noise. Using (2.18), the location angle of target can be found as

$$\theta_p = \sin^{-1}\left(\frac{1}{\pi}\tan^{-1}\left(\frac{x_1x_2 + y_1y_2}{x_2y_1 - x_1y_2}\right)\right). \tag{2.19}$$

The phase value of the car present at some particular range can be used to know if the target is entering or exiting the parking slot. If a car is entering into the parking

slot, the phase will increase or decrease in consecutive frames, while if a car is exiting the parking slot, the phase will change in the opposite direction. This phase value can also know if the vehicle is not properly parked in the parking slot. In this case, the phase value will be greater than some predefined threshold value, and it will not change from one frame to the other.

The limitation associated with this technique is that if the height of the car parked in front of the radar is higher than the cars parked after it, this can block the radar field-of-view. In this case, the peaks from such cars will be very weak, and as a consequence, our proposed algorithm can show occupied parking slots as available parking slots. One solution to this problem can be to increase the height of radar height. This solution is suitable for open parking. However, in indoor parking, height is limited, and this is not the option. Because the radar cannot be deployed at a very high altitude, the blockage effect will be particularly noticeable. Besides, there are many obstacles and the reflections from them will confuse the processor. So we need an adaptive threshold maker to overcome the above issues, in the next chapter, a background recording-based technique is proposed.

2.4 CFAR Algorithm

Generally, the signal is emitted by the signal source, which is subjected to various interference in the process of transmission. After reaching the receiver, it is processed and output to the detector, which then makes a decision on the input signal according to the appropriate criteria. The constant false alarm detector firstly determines a threshold after processing the input noise and compares this threshold with the input signal. If the input signal exceeds this threshold, it is judged as having a target; otherwise, it is judged as having no target.

So the received signal can be expressed as

$$y = h \cdot x + n. \tag{2.20}$$

h can be equal to 0 or 1, which means the transmitted signal exist or really exists, respectively. H_0 and H_1 are two hypothesises representing the target exists or not exist. D_0 and D_1 are two facts representing the target exists or not exist. According to the combination of H and D, we can get three kinds of results: correct detection, false dismissal and false alarm. Fig. 2.2 shows how different results are produced.

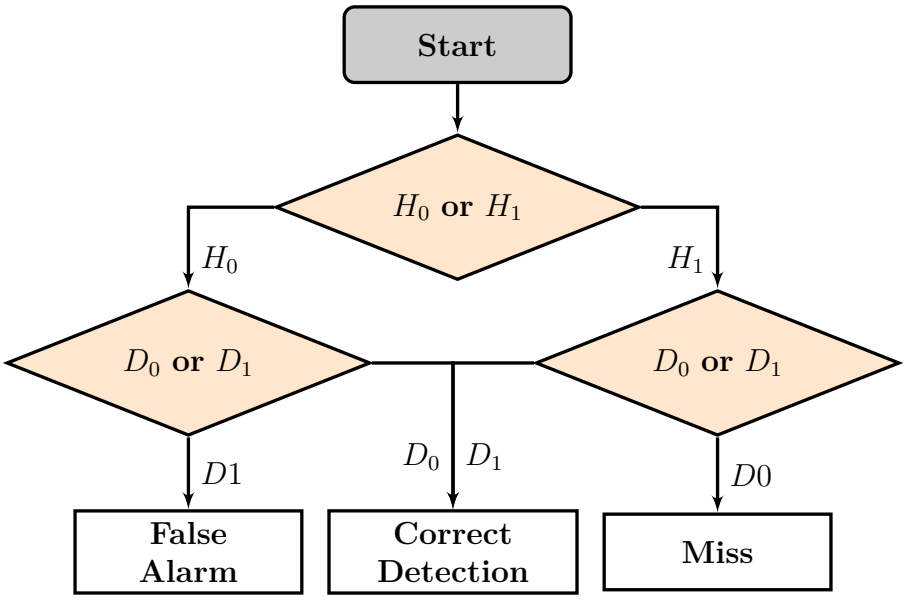

Figure 2.2: Correct detection is result from two cases: H_0 is true and D_0 is true, or H_1 is true and D_1 is true. False dismissal means H_1 is true and D_0 is true. False alarm means H_0 is true and D_1 is true. CFAR algorithm is proposed to avoid false alarm.

Suppose $p(z|H_0)$ and $p(z|H_1)$ represent the probability density function (PDF) of the received signal under hypothesis H_0 and H_1. Suppose the threshold is θ. If the level of the received signal is greater than θ, the detector determines there is a target, and vice verse. The idea of CFAR is to determine the probability of false alarm firstly, then try to minimize the probability of false dismissal. Suppose P_F and P_M represent

the probability of false alarm and false dismissal, respectively. Equ. 2.21 illustrates this optimization problem.

$$\begin{aligned} \min \quad & P_M, \\ \text{s.t.} \quad & P_F = \alpha, \end{aligned} \tag{2.21}$$

where α is the chosen probability of false alarm. Using Lagrangian multiplier method,

$$\begin{aligned} J &= P_M + \lambda(P_F - \alpha), \\ &= \int_0^\theta p(z|H_1)dz + \lambda[\int_\theta^\infty p(z|H_0)dz - \alpha], \\ &= \int_0^\theta p(z|H_1)dz + \lambda[1 - \int_0^\theta p(z|H_0)dz - \alpha], \\ &= \lambda(1-\alpha) + \int_0^\theta [p(z|H_1) - \lambda p(z|H_0)]dz. \end{aligned} \tag{2.22}$$

Let the derivative of J with respect to θ be zero,

$$\lambda(\theta) = \frac{p(\theta|H_1)}{p(\theta|H_0)}. \tag{2.23}$$

Let define the likelihood ratio as Equ. 2.24

$$\lambda(z) = \frac{p(z|H_1)}{p(z|H_0)}. \tag{2.24}$$

Thus, we can calculate the corresponding likelihood ratio from the level of the received signal. If $\lambda(z) > \lambda(\theta)$, the detector determines there is a target. Otherwise there is none.

Example 2.4.1. The source output voltage is 1 when a signal is being transmitted, 0 otherwise. Suppose the channel is additive White Gaussian noise (AWGN) channel with zero mean value and variance 1. Compute the corresponding probability of correct detection and the threshold of likelihood ratio with $P_F = 0.1$

Suppose the received signal is z and the noise is n. So H_0 and H_1 can be expressed as

$$H_1 \quad : z = 1 + n, \tag{2.25}$$

$$H_0 \quad : z = n. \tag{2.26}$$

The PDF of n is

$$p_N(n) = \frac{1}{\sqrt{2\pi}}\exp(-\frac{n^2}{2}). \tag{2.27}$$

So the PDF of H_0 and H_1 are

$$p(z|H_0) = \frac{1}{\sqrt{2\pi}}\exp(-\frac{z^2}{2}), \tag{2.28}$$

$$p(z|H_1) = \frac{1}{\sqrt{2\pi}}\exp(-\frac{(z-1)^2}{2}). \tag{2.29}$$

$$\tag{2.30}$$

So the likelihood ratio is

$$\lambda(z) = \frac{p(z|H_1)}{p(z|H_0)} = \exp(z - \frac{1}{2}). \tag{2.31}$$

Suppose the threshold of the level of the received signal is θ. Because $P_F = 0.1$,

$$\int_\theta^\infty p(z|H_0)dz = \int_\theta^\infty \frac{1}{\sqrt{2\pi}}\exp(-\frac{z^2}{2})dz = 0.1. \tag{2.32}$$

The root is

$$\theta = 1.29. \tag{2.33}$$

So the threshold of likelihood ratio is

$$\lambda(\theta) = \exp(\theta - \frac{1}{2}) = 2.2. \tag{2.34}$$

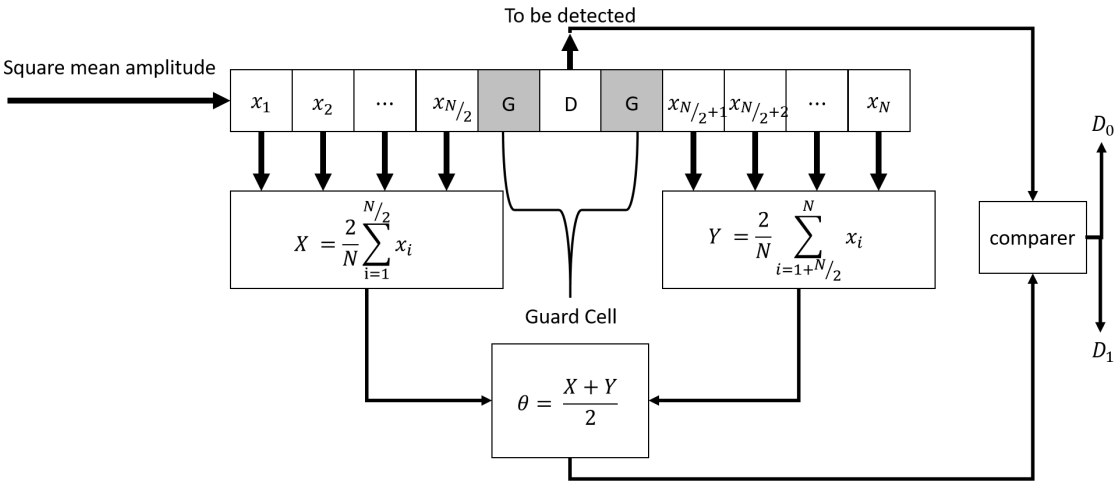

Figure 2.3: Except guard cells, The mean square amplitude of a certain number of adjacent sampling points is calculated. They are called training cells. In our practice, there are guard cells and training cells on both sides. The level of the cell to be detected will be compared with the mean square amplitude of training cells to determine whether there is really a target.

and the probability of correct detection is

$$P_D = \int_\theta^\infty p(z|H_1)dz = \int_\theta^\infty \frac{1}{\sqrt{2\pi}}\exp[-\frac{(z-1)^2}{2}]dz = 0.614. \tag{2.35}$$

In our scenario, we use cell-averaging CFAR (CA-CFAR) which uses the mean square amplitude of other sampling points around the cell to be detected as the detection criterion. The diagram of this algorithm is shown in Fig. 2.3. The data flow will be sampled and divided into four categories: to be detected cell, training cells, guard cells and irrelevant cells. The cell to be detected is D in Fig. 2.3, training cells are x in Fig. 2.3, and guard cells are G in Fig. 2.3. The mean square amplitude of x will be calculated and is represented as θ in Fig. 2.3. θ is the threshold. Then it will be compared with the level of D. if $D > \theta$, the result will be D_1. Otherwise it will be D_0. G is the cells that are near to D and the number of G is called guard width. To enhance accuracy, the level of G isn't used. Usually, the channel is AWGN channel. So we are going to derive the closed expression of θ subject to a given P_F.

Firstly, let $X_1, \ldots, X_k$ be k independent and normally distributed random variables and suppose

$$x = \sum_{i=1}^{k} X_i^2. \tag{2.36}$$

Thus, x is a Chi-squared distributed (χ_2- distribution) variable of k degrees-of-freedom and the PDF is

$$p(x,k) = \frac{1}{2^{k/2}\Gamma(k/2)} x^{k/2-1} \exp(-x/2). \tag{2.37}$$

Furthermore, suppose X_i satisfy

$$\begin{aligned} E[X_i] &= \mu_i, \\ \sigma_i^2 &= 1. \end{aligned} \tag{2.38}$$

then according to non-central Chi-squared distribution, the simplified PDF of x is

$$p(x,k,\lambda) = \frac{1}{2}\left(\frac{x}{\lambda}\right)^{k/4-1/2} \exp\left(-\frac{x+\lambda}{2}\right) I_{k/2-1}(\sqrt{\lambda x}). \tag{2.39}$$

where $I_p(y)$ is the modified Bessel function of the first kind, and

$$\lambda = \sum_{i=1}^{k} \mu_i^2, \tag{2.40}$$

which is called a non-centrality parameter.

Then we can derive the closed expression of P_F.

$$\begin{aligned} P_F &= \int_T^\infty p(x|H_0)dx, \\ &= \frac{1}{\sqrt{2\sigma^2}} \int_T^\infty \exp(-\frac{x^2}{2\sigma^2})dx, \\ &= \frac{1}{2}\text{erfc}\left(\frac{T}{\sqrt{2\sigma^2}}\right). \end{aligned} \tag{2.41}$$

Given a certain $P_F = \epsilon$, the threshold of the level of the received signal is

$$T = \sqrt{2\sigma^2}\text{erfc}^{-1}(2\epsilon). \tag{2.42}$$

In our scenario, square law is used in our modulation/demodulation. So the sampled signal is the sum of the squares of the amplitudes of in-phase and quadrature-phase components. The probability distribution function of the sampled signal becomes a chi-squared distributed of the degree-of-freedom of 2. In the amplitude detector the sampled signal is the square-root of the sum of the squares of the amplitudes of in-phase and quadrature-phase components. In this case, the probability distribution function of the sampled signal becomes a Rayleigh faded.

For square-law detector, if no signal is transmitted, the PDF of the received signal is

$$p(x|H_0) = \frac{1}{2\sigma^2}\exp(-\frac{x}{2\sigma^2}). \tag{2.43}$$

So P_F can further reduced to

$$\begin{aligned} P_F &= \int_T^\infty p(x|H_0)dx, \\ &= \frac{1}{2\sigma^2}\int_T^\infty \exp(-\frac{x}{2\sigma^2})dx, \\ &= \frac{1}{2\sigma^2}\frac{e^{-x/2\sigma^2}}{-1/2\sigma^2}\Big|_T^\infty, \\ &= \exp(-\frac{T}{2\sigma^2}). \end{aligned} \tag{2.44}$$

Given a certain $P_F = \epsilon$, the threshold of the level of the received signal is

$$T = -2\sigma^2 ln(\epsilon). \tag{2.45}$$

To find the value of T, noise power is required.If the actual noise power is more than the assumed one, the P_F will increase, and vice verse. To tackle this problem noise

Table 2.1: Parameters in recording raw data. FFT means Fast Fourier Transform.

Frame interval/s	0.5
Up-Chirp duration/μs	300
Chirp bandwidth/MHz	150
Number samples per chirp	128
Number chirps per frame	16
Carrier frequency/GHz	24
FFT points	1024
False alarm probability	0.001
Training cell length	24
Guard width	1

power is estimated for each range bin using the nearby samples, and this idea has been shown in Fig 2.3. To sum up, CFAR adaptively change the threshold value to keep the P_F constant. And that's where it got its name.

2.5 Preliminary results

In this section, we'd like to show some preliminary results from our raw data. we will reveal the difference between the data collected with and without cars. Then we will see how CFAR helps us to eliminate the interference from obstacles.

Table. 2.1 shows the parameters we used in recording raw data. According to 2.14, the range step in frequency domain is 0.125m. From the distance measured in our experiment field, the width of each parking slot is about 3m. So there are 24 sample points for each parking slot. Thus, we let the training cell length to be 24 which means fully considering adjacent two parking slots in both sides.

Fig. 2.4 shows the spectrum of one of the frames recorded from our experiment site. Fig. 2.5 shows the optical reference of Fig. 2.4. From Fig. 2.5, we can clearly see there is a black sedan in the third parking slot. According to our measurements, the sedan is approximately 8.75 meters from the radar. We can find the corresponding peak in Fig. 2.4. Meanwhile, except this main peak, there are also many pipes in the ceiling and pillars. they can be the reason for other weak peaks. Sidelobe leakage is

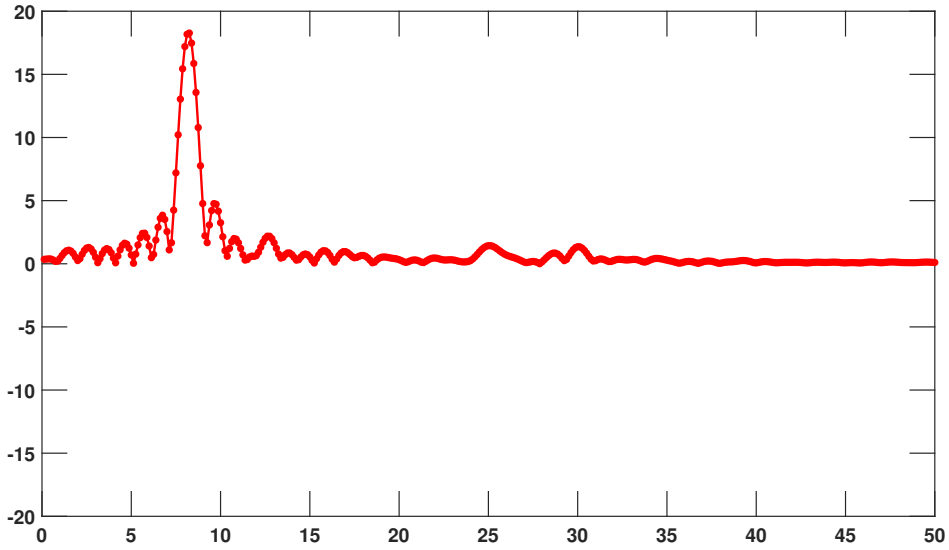

Figure 2.4: There is one car in 8.75m which is also the location of the third parking slot. And that corresponds to the peak in the figure. However, there are also other small peaks and impulses. They result from obstacles such as pillars and pipes and sidelobe leakage.

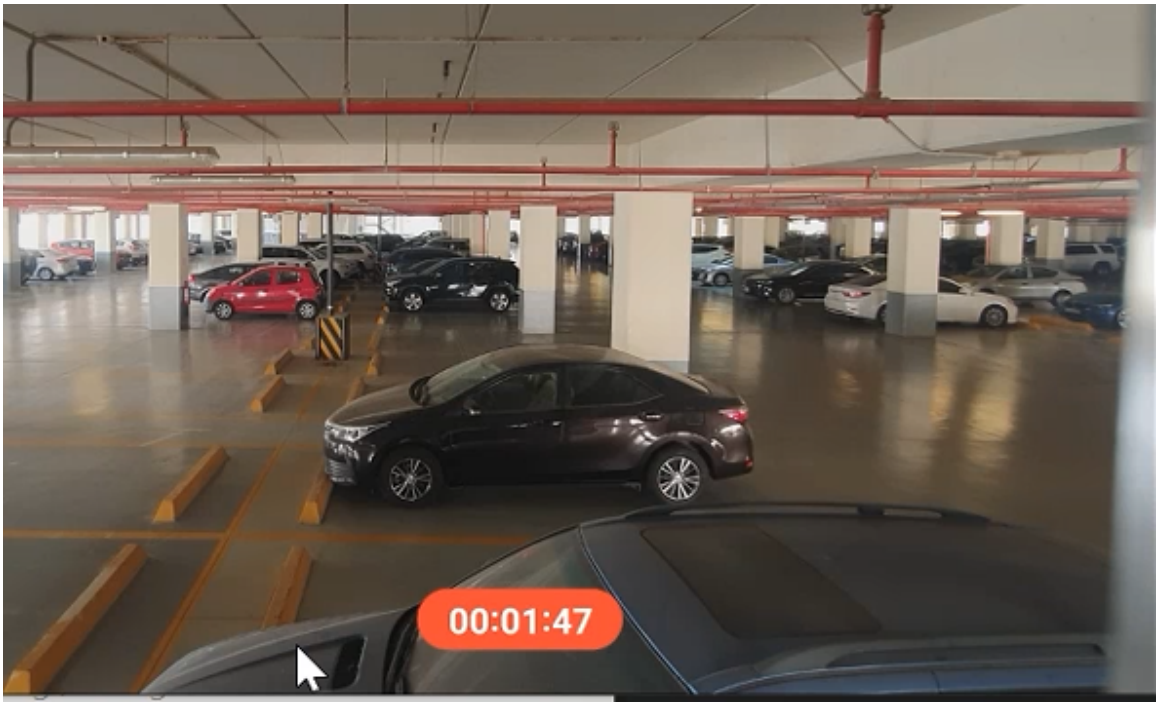

Figure 2.5: The optical reference of Fig. 2.4

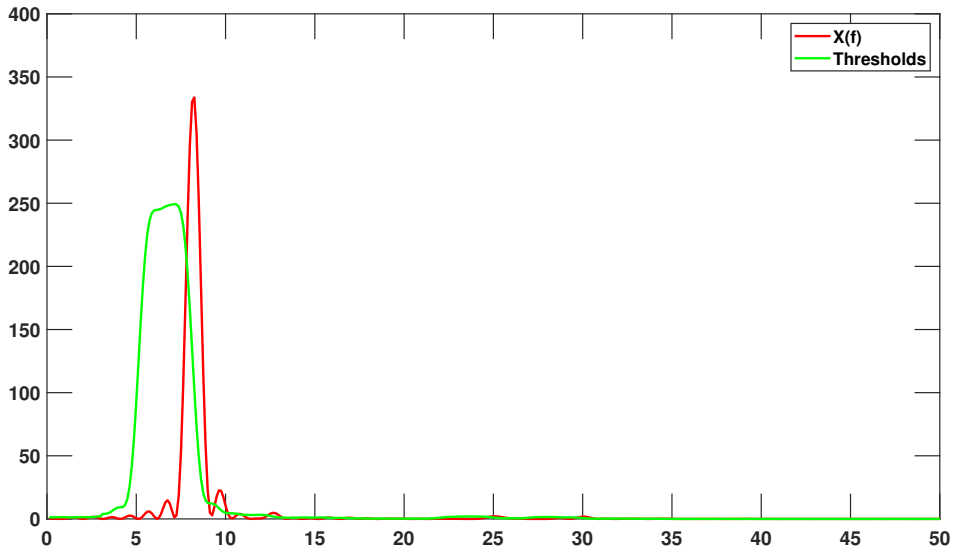

Figure 2.6: The red line is the amplitude spectrum of Fig. 2.4 and the green line is the corresponding thresholds given by CFAR. Many peaks are considered as obstacles because of their low level.

another cause of spectral unsmoothness. Because we don't know the number of cars in the field, the radar cannot easily distinguish cars from these peaks. But usually the reflection from cars are much more stronger than pillars and pipes, so CFAR can adaptively give us thresholds. Fig. 2.6 shows the results by applying CFAR. we can find cars by the following three steps: (1) Use radar to record data. (2) Apply FFT and CFAR. (3) Compare the level of sampling points and thresholds.

Chapter 3

Background Subtraction-based Algorithm

3.1 Introduction

In Chapter. 2, we depicts the three steps for monitoring parking lots. It is enough for big and empty outdoor parking lots. But actually obstacles and sidelobe leakage are two remaining problems. Note that many obstacles such as pipes and pillars are stationary so we can always receive the similar signal from them. So if we subtract the data of the previous frame from the data of the later frame, we can eliminate the interference of the obstacles. Besides, this background subtraction idea can also overcome blockage effect. Because if a car parks in a specific parking slot, then it probably won't move again for quite some time. So this parked car can be considered as background noise. Thus, it cannot block the other cars which want to park later on because the signal from the parked car will be eliminated. For sidelobe, we applied windowing function and summing average of all chirps. The advantages of this method are simple and low complexity, so it can be applied to our online experiment.

The organization of this chapter is as follows. In Sec. 3.2, we discussed the detail steps and key component to solve the sidelobe leakage and background noise. Sec. 3.3 explains our algorithm which is suitable for both outdoor and indoor parking. Performance analysis of the monitoring system after applying our proposed algorithm is discussed in Sec. 3.4.

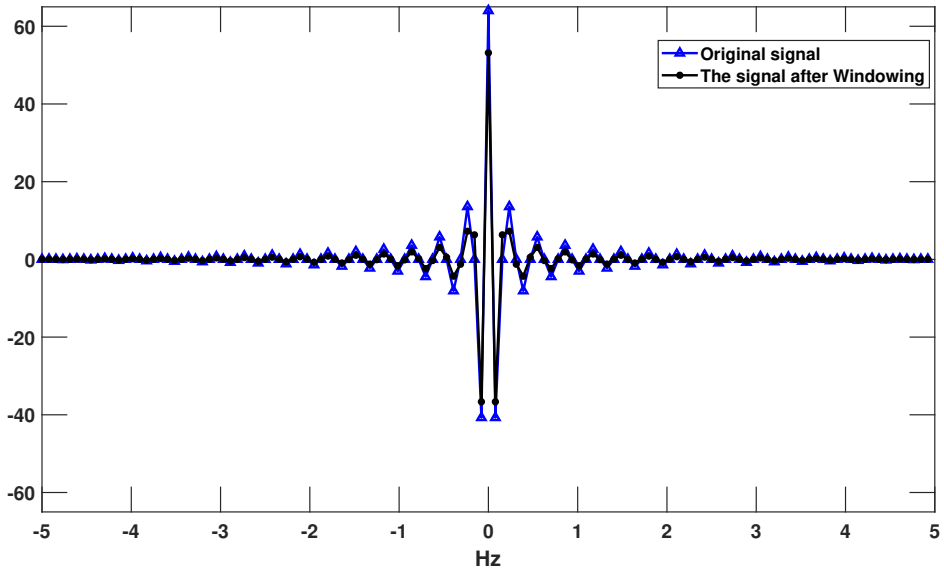

Figure 3.1: The effect of Hamming windowing function. The envelope reduced clearly comparing with the original signal

.

3.2 Solution for sidelobe leakage and background noise

Windowing function can significantly help us reduce the amplitude of sidelobe leakage. Here, we applied Hamming function whose length is 128. Fig. 3.1 shows how this Hamming function suppress the sidelobe of $y(t) = rect(t)$.

$$y(t) = rect(t) = \begin{cases} 0 & |t| > \frac{1}{2} \\ \frac{1}{2} & |t| = \frac{1}{2} \\ 1 & |t| < \frac{1}{2} \end{cases} \tag{3.1}$$

Besides, although the sidelobe leakage could not be eliminated by averaging, we still sum and average the sampling points of all 16 chirps. Actually background noise is very low and the environment is almost stationary. So the influence of noise can be ignored after averaging. Fig. 3.2 shows the comparison of multiple signal from different source.

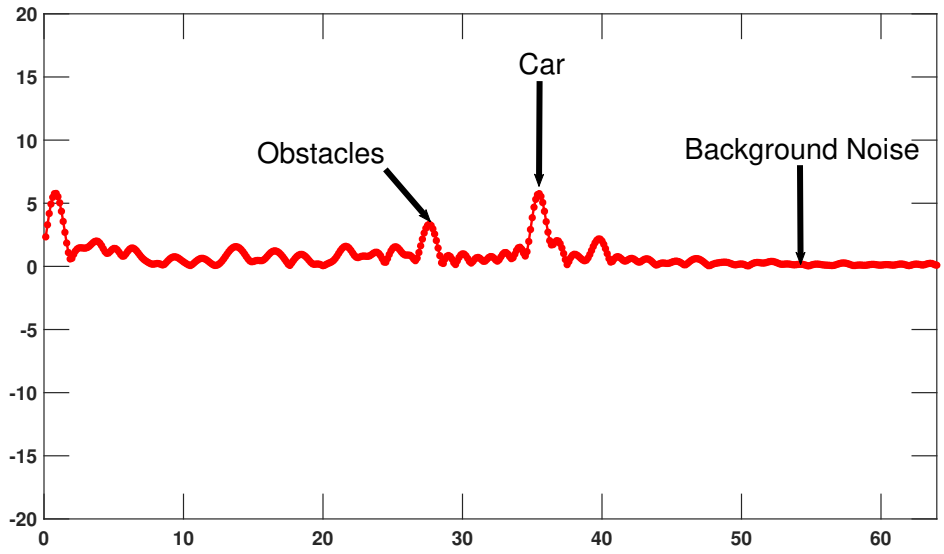

Figure 3.2: The Signal power varies widely from different sources. The noise power is very weak and can be ignored. The reflection of obstacles such as pillars and pipes are closer than a car if the car is parked far away.

3.3 The steps of background subtraction-based algorithm

Fig. 3.2 shows it is not enough to distinguish a car only using averaging, windowing and CFAR. Environment obstacles are the most severe challenge. Ideally, when a vehicle is moving, only a single, distinct peak appears in the spectrum. Note that the environment obstacles are almost stationary. Vehicles cannot completely block big pillars and pipes because they are tall and huge. So they give approximate feedback on each frame. Thus, they can eliminated by calculating the difference between two frames. Besides, a car can be seen as an obstacle is it has been parked. Therefore, the blocking effect between vehicles can also be eliminated by this way. The processor only process the new frame representing the difference between two frames. Only moving targets, which are cars in our scenario, can be clearly seen in this new frame. In the following, three different scenarios are considered. In the first and second scenarios, only one car enters and exits the parking slot at a time, while in the third scenario, more than one cars can enter and exit the parking slot. In the first

scenario, entering or exiting a car does not block the radar field of view. In the second scenario, the radar field of view is partially blocked. In the third scenario, more than one cars can enter and exit the parking slots. In all of the proposed techniques, the time domain received signals are transformed into the frequency domain, and only frequency domain signals are used in the processing.

3.3.1 Unblocked Radar Field-of-View

For a radar, indoor environment is very challenging due to clutter (received signal due to unwanted scatterers present in the environment). For a fixed radar in an indoor environment, target free received signal can be written as

$$r(t) = r_L(t) + r_B(t), \tag{3.2}$$

where $r_L(t)$ and $r_B(t)$ respectively represent leakage (received signal due to the internal circuitry) and background (clutter) signals and generally don't change with respect to time. Therefore, the overall received signal in the presence of the target can be written as

$$x(t) = y(t) + r(t),$$

where $y(t)$ is defined in (2.2) and contains the signal and noise components. Above equations are approximately valid when the background return is essentially unaffected by the presence of the targets. In fact, subtracting $r(t)$ in (3.2) from $x(t)$ can significantly improves the detection performance.

In FMCW radar, the frequency-domain received signal shows a peak corresponding to each target present in the radar field-of-view. Our proposed technique dedicates a memory location for each parking slot. If in a parking slot, a vehicle is present, the corresponding memory location is assigned one; otherwise, zero. Moreover, the

proposed technique assumes the presence of a background signal (BS) before processing a new received signal. The proposed algorithm receives a signal, subtracts the BS from it, and updates the BS with the received signal. Consider frequency-domain background and received signals are respectively denoted by $B(f)$ and $Z(f)$, while the background and received signal values at peak corresponding to ith parking slot are respectively denoted by $B(f_i)$ and $Z(f_i)$. The BS subtraction from the received signal at peak i can be written as

$$|Z(f_i)| - |B(f_i)| = \Delta(f_i). \tag{3.3}$$

Adaptive thresholds is given by applying CFAR to the power spectrum of $Z(f)$ and $B(f)$. Suppose $\eta(f_i)$ is the positive threshold value given by CFAR. If $\Delta(f_i) \geq \eta(f_i)$, our proposed algorithm assigns 1 to the ith memory location to show parking slot is occupied, and if $\Delta(f_i) \approx 0$, proposed algorithm does not change the memory status. On the other hand, if the subtraction of BS from the received signal produces a peak and $\Delta(f_i) \leq -\eta(f_i)$, the system assign 0 to the ith memory location to show parking slot is available. The flowchart of the algorithm is shown in Fig. 3.3.

To show the working of the proposed algorithm, Fig. 3.4 describes few scenarios for three parking slots. Initially, we assume all parking slots are available and save the corresponding received signal as BS and initialize $\eta(f_i)$ for $i = 1, 2, 3$. As shown in the figure, a car enters the first parking slot in the first state. The received signal yields a peak corresponding to the 1st parking slot, and $\Delta(f_1) \geq \eta(1)$. In this case, the system updates the BS with the received signal and assigns 1 to the first memory location. If in the next state received signal does not change, $\Delta(f_1) \approx 0$ and for $\forall i \geq 1$. In this case, the system updates the BS but does not change the memory status. In the second state, when a car enters the 2nd parking slot, the received signal yields two peaks corresponding to the 1st and 2nd parking slots. The BS subtraction

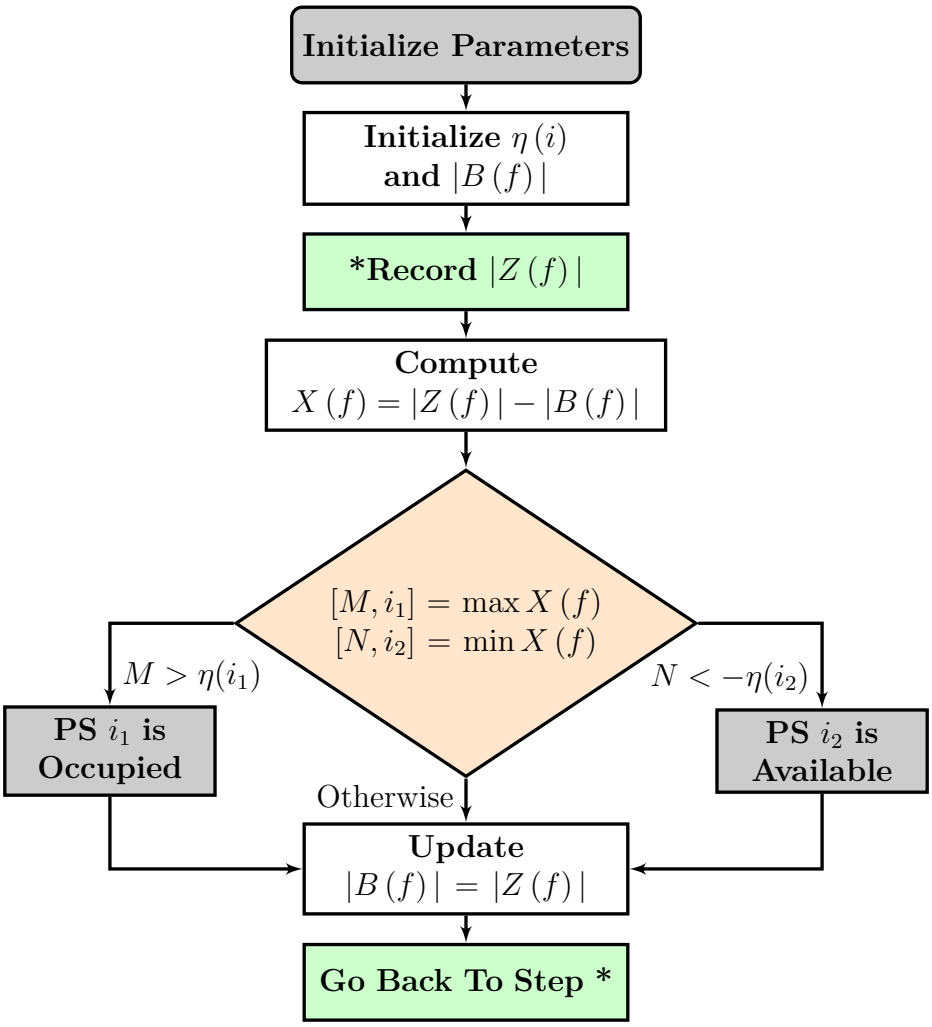

Figure 3.3: Proposed algorithm flow chart when a car does not block radar FoV, where PS stands for parking slot and the values of $\eta(i_1)$, $\eta(i_2)$ inversely proportional to the range.

from the received signal yields a peak corresponding to the 2nd parking slot and $\Delta(f_2) \geq \eta(f_2)$. In this case, the system updates BS with the received signal and assigns 1 to the 2nd memory location. Similarly, when a car enters the 3rd parking slot in the third state, the received signal yields three peaks corresponding to the 1st, 2nd, and 3rd parking slots. In this case, the BS subtraction from the received signal yields a peak corresponding to the 3rd parking slot, and $\Delta(f_3) \geq \eta(f_3)$. Like previous cases, the system updates BS with the received signal and assigns 1 to the 3rd memory location. In the fourth state, a car leaves the 3rd parking slot, and the received signal shows only two peaks corresponding to the 1st and 2nd parking slots. Since the BS has three peaks, the BS subtraction from the received signal yields only one peak at the 3rd location. In this case, $\Delta(f_3) \leq -\eta(f_3)$, therefore, the proposed algorithm assigns 0 to the memory location corresponding to the 3rd parking slot and updates BS with the received signal. The output in the remaining states follows the same strategy.

3.3.2 Blocked Radar Field of View

In the above section, cars were entering and exiting the parking slots, but none blocked the radar FoV to see other cars. In this section, we will discuss more complex scenarios. If a car blocks radar FoV, the above technique needs to be modified. In such cases, the BS subtraction from the received signal can generate more than one peak. If a car enters into a parking slot p and blocks the radar FoV to see other cars, the BS subtraction from the received signal at peaks corresponding to a vehicle in parking slot i can be written as

$$\begin{aligned} \Delta(f_i) &= 0, \text{ for } \quad i < p \\ &= -\epsilon, \qquad i > p \\ &= \beta, \qquad i = p \end{aligned} \tag{3.4}$$

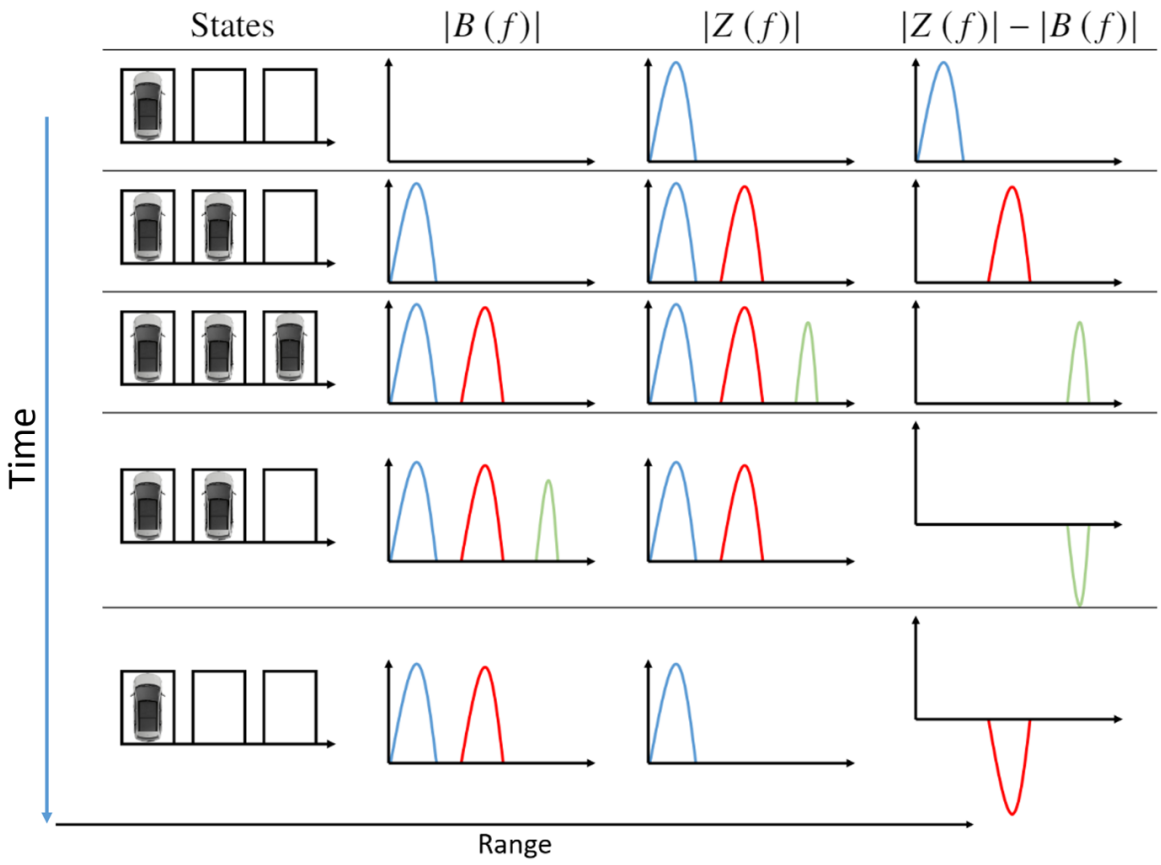

Figure 3.4: Entering or exiting car does not block the radar FoV and one car moves at a time. In such scenario the BS subtraction from received signal generates only one peak.

where $\epsilon > 0$ is a small number, its value depends on the FoV blocking, and $\beta \gg 0$. If the entering car does not block the radar FoV $\epsilon = 0$. Similarly, if a car leaves a parking slot p and it was blocking the radar FoV to see other cars, the BS subtraction from the received signal at peaks corresponding to a vehicle in parking slot i can be written as

$$\begin{aligned} \Delta(f_i) &= 0, \text{ for } \quad i < p \\ &= \epsilon, \qquad\quad i > p \\ &= -\beta, \qquad i = p. \end{aligned} \tag{3.5}$$

Our proposed algorithm exploits the above facts to know if a parking slot is available or occupied. Since the BS subtraction from the received signal before the entering or exiting location will be equal to zero, the positive peak at pth location will represent the presence of a car. In contrast, the negative peak will represent the absence of a car or a parking slot is available. Our proposed algorithm ignores all peaks after parking location p. In other words, the first peak of the spectrum of BS subtraction from the received signal, if greater than the predefined threshold $\eta < \beta$, represents the entering or exiting parking slot. Since we look for only the 1st peak in the

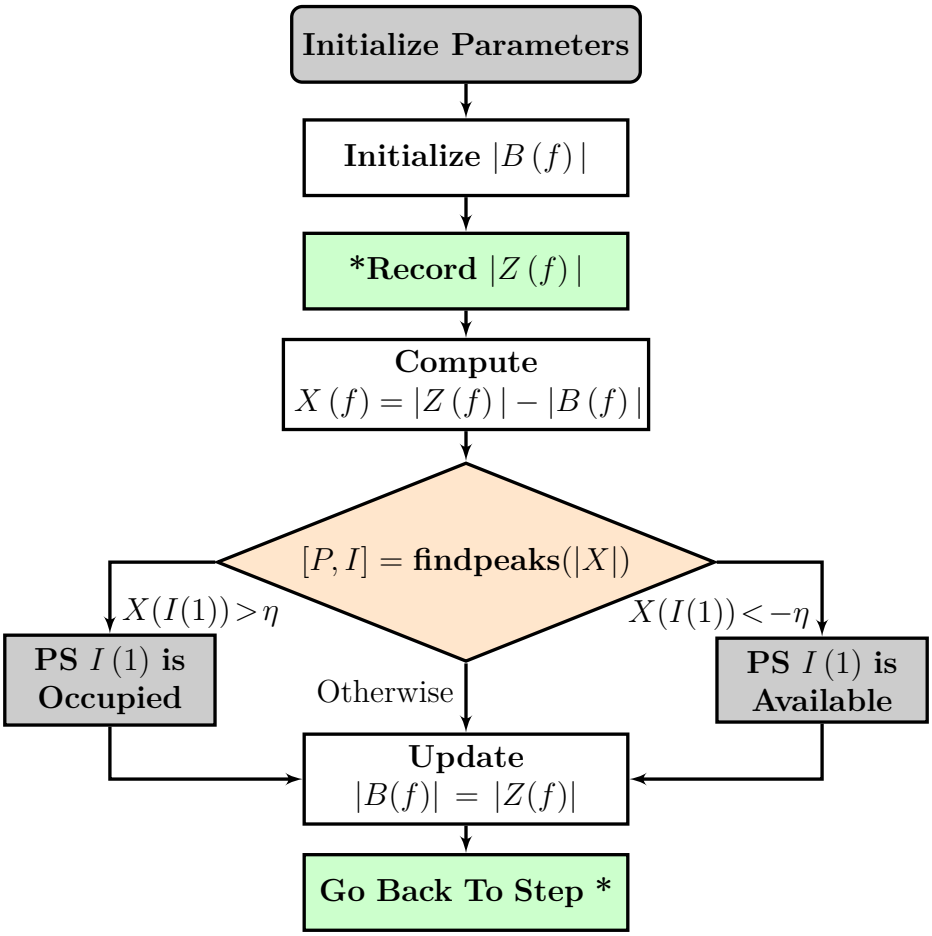

Figure 3.5: Proposed algorithm flowchart when entering or exiting car blocks the radar FoV but one car moves at a time.

proposed algorithm, there is no need to define threshold values for different parking slots. One small threshold value is enough for all locations. The flowchart of the

algorithm is shown in Fig. 3.5.

Fig. 3.6 describes different scenarios. In the first state, a car enters the 3rd parking slot in a completely free parking lot. The received signal yields a peak corresponding to the 3rd parking slot, and $\Delta(f_3) \geq \eta$, while $\Delta(f_i) \approx 0$ for $i \leq 3$. In this case, the proposed algorithm assigns 1 to the memory location corresponding to 3rd parking slot to show parking slot is occupied, and updates the BS with the received signal. In the second state, a car enters the 2nd parking slot and partially block the radar FoV to see a car in 3rd parking slot. Now, the received signal yields two peaks corresponding to the 2nd and 3rd parking slots. It should be noted that the peak due to a car in 3rd parking slot has decreased due to the radar FoV blocking. In this case, $\Delta(f_2) = \beta > \eta$, $\Delta(f_i) \approx 0$ for $i < 2$, and $\Delta(f_i) = -\epsilon$ for $i > 2$. Since the first peaks occur at 2nd parking slot location and is positive, the proposed algorithm assigns 1 to the memory location corresponding to the 2nd parking slot and updates the BS with the received signal. Similarly, a car enters the 1st parking slot in the third state and partially blocks the radar FoV to see cars in the 2nd and 3rd parking slots. The received signal yields three peaks corresponding to the 1st, 2nd, and 3rd parking slots. Observe that the peaks corresponding to 2nd and 3rd parking slots have decreased due to the radar FoV blocking by the first car. In this case, $\Delta(f_1) = \beta > \eta$, and $\Delta(f_i) = -\epsilon$ for $i > 1$. Since the 1st peak corresponds to the 1st parking slot location and is positive, the proposed algorithm assigns 1 to the memory location corresponding to the 1st parking slot and updates the BS with the received signal. In the fourth state, a car leaves the 1st parking slot. Since it was partially blocking the radar FoV to see 2nd and 3rd parking slots, the peaks corresponding to these cars will slightly increase in the received signal. In this case, the received signal yields two peaks corresponding to the 2nd and 3rd parking slots. Now, $\Delta(f_1) = -\beta < -\eta$, and $\Delta(f_i) = \epsilon$ for $i > 1$. Since the 1st peak corresponds to the 1st parking slot and is negative, the proposed algorithm assigns 0 to the memory location corresponding to

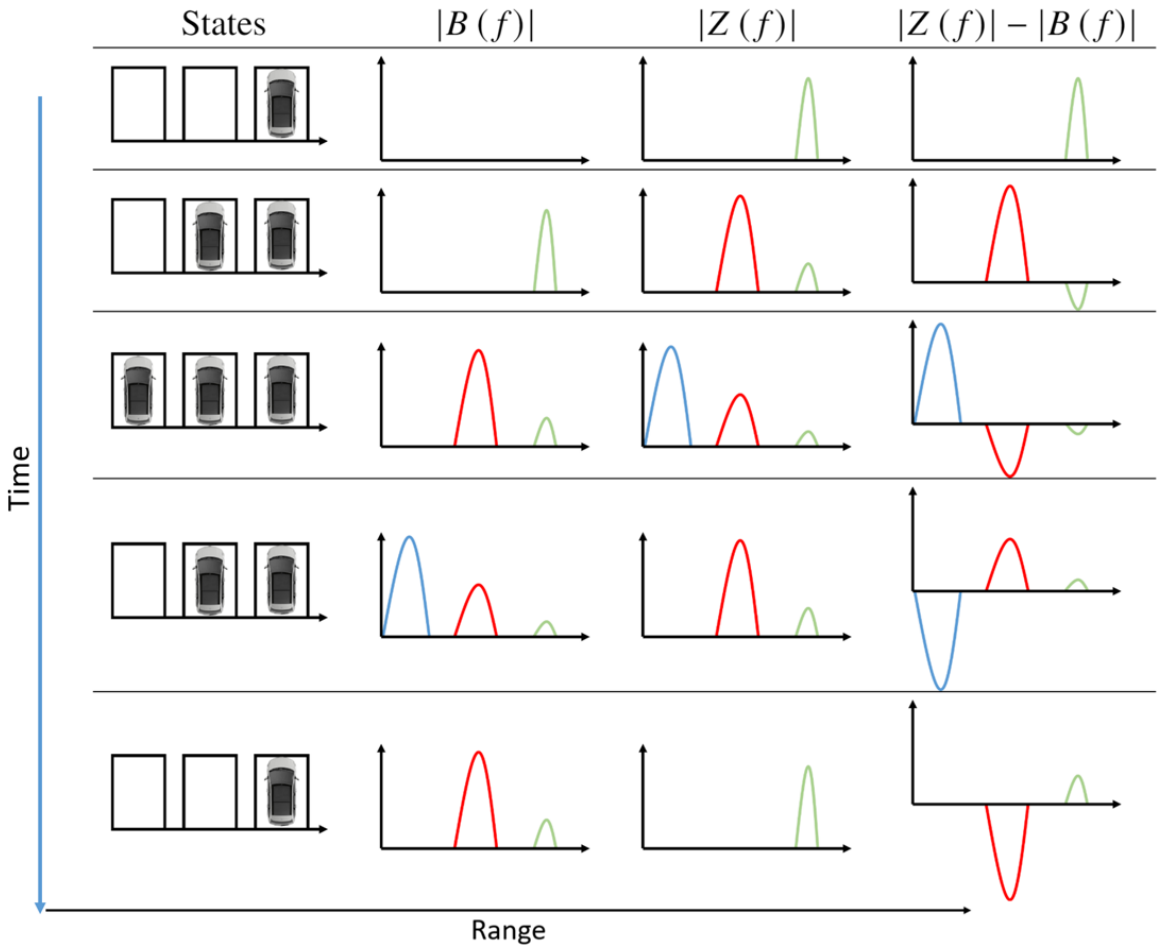

Figure 3.6: Entering or exiting car blocks the radar FoV and one car moves at a time. In such scenario the BS subtraction from received signal can generate more than one peak.

the 1st parking slot to show the parking slot is available and updates the BS with the received signal. Other states follow the same strategy.

3.3.3 Cars Block Radar Field of View and Multiple Cars Enter and Exit

In both of the above subsections, only one car enters or exits the parking lot at one time. If more than one car enters or exits the parking slot, such a situation can generate more than one prominent peak, along with the peaks that occur due to the radar FoV blocking. For example, consider a background in which three cars are

Table 3.1: When a vehicle enters, leaves and remains at rest, the spectral sampling point has a different magnitude relationship to the threshold. By using CFAR for B, Z, and X respectively, the motion of the vehicle can be determined.

Cars are entering	$\|B(f_i)\| < \theta_1, \|Z(f_i)\| > \theta_2, \|X(f_i)\| > \theta_3, X(f_i) > 0$
Cars are leaving	$\|B(f_i)\| > \theta_1, \|Z(f_i)\| < \theta_2, \|X(f_i)\| > \theta_3, X(f_i) < 0$
Cars didn't move	$\|B(f_i)\| > \theta_1, \|Z(f_i)\| > \theta_2$

occupying parking slots. The first car partially blocks the radar FoV to see 2nd and 3rd cars. Suppose 1st and 3rd cars exit the parking slots. Exiting the 1st car increases the amplitude of the 2nd car. Therefore, the BS subtraction from the received signal yields prominent negative, weak positive, and weak negative peaks respectively at 1st, 2nd, and 3rd locations. In such a scenario, it becomes challenging to decide the cause of the 2nd and 3rd peaks. However, if a car exit the parking slot, its corresponding peak in the received signal becomes negligible on average. Using this fact, in the following, we use CFAR to generate three thresholds $\theta_1, \theta_2, \theta_3$, to determine if the car is entered or exited the parking slot i. $\theta_1, \theta_2, \theta_3$ are thresholds for $B(f), Z(f)$, and $X(f)$, respectively. Table. 3.1 shows how the spectrum should behave when a vehicle is entering, leaving, or keeping stationary. Our proposed algorithm, exploits these facts to decide if the parking slot is occupied or available. The flowchart of the algorithm is shown in Fig. 3.7.

This scheme can be consider as a generalized for the above two cases in Sec. 3.3.1 and 3.3.2. Few scenarios are shown in Fig. 3.8. In the first state, two cars enters the 1st and 2nd parking slots in a completely free parking lot. The received signal yields two peaks corresponding to the 1st and 2nd parking slots. For the sampling point corresponding to the first parking space, firstly there is no peak in $|B(f)|$, then a peak occurs in $|Z(f)|$. In addition, a positive peak also occurs in $|Z(f)| - |B(f)|$. According to Table. 3.1, a car is entering the 1st parking slot. We can conclude a car is entering the 2nd parking slot in the same way. In the second state, a car leaves 1st parking slot and another car enters the 3rd parking slot. Now, the received signal

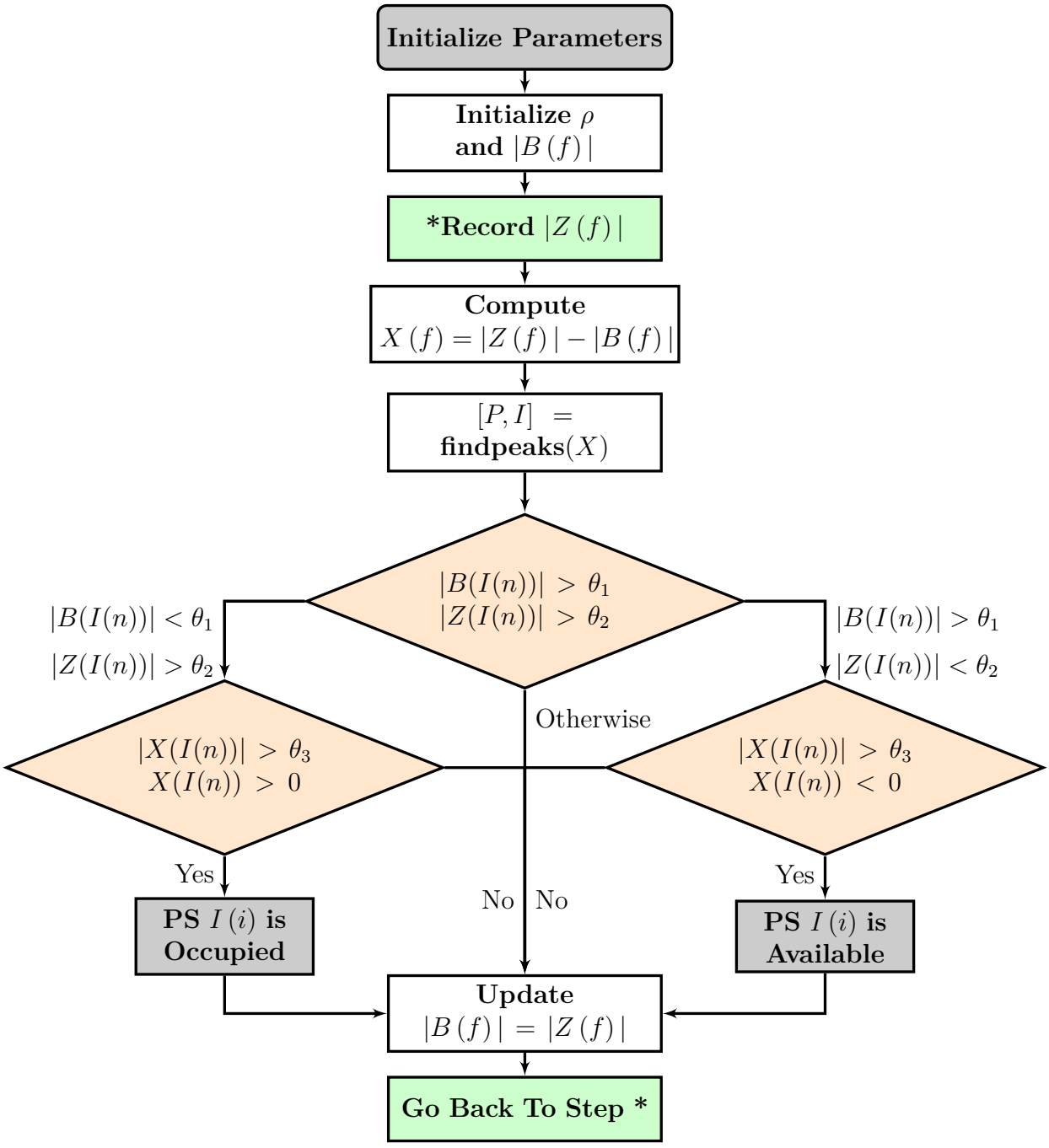

Figure 3.7: Generalized proposed algorithm flowchart for anti-blocking and multiple car movement detection, where ρ is a threshold value.

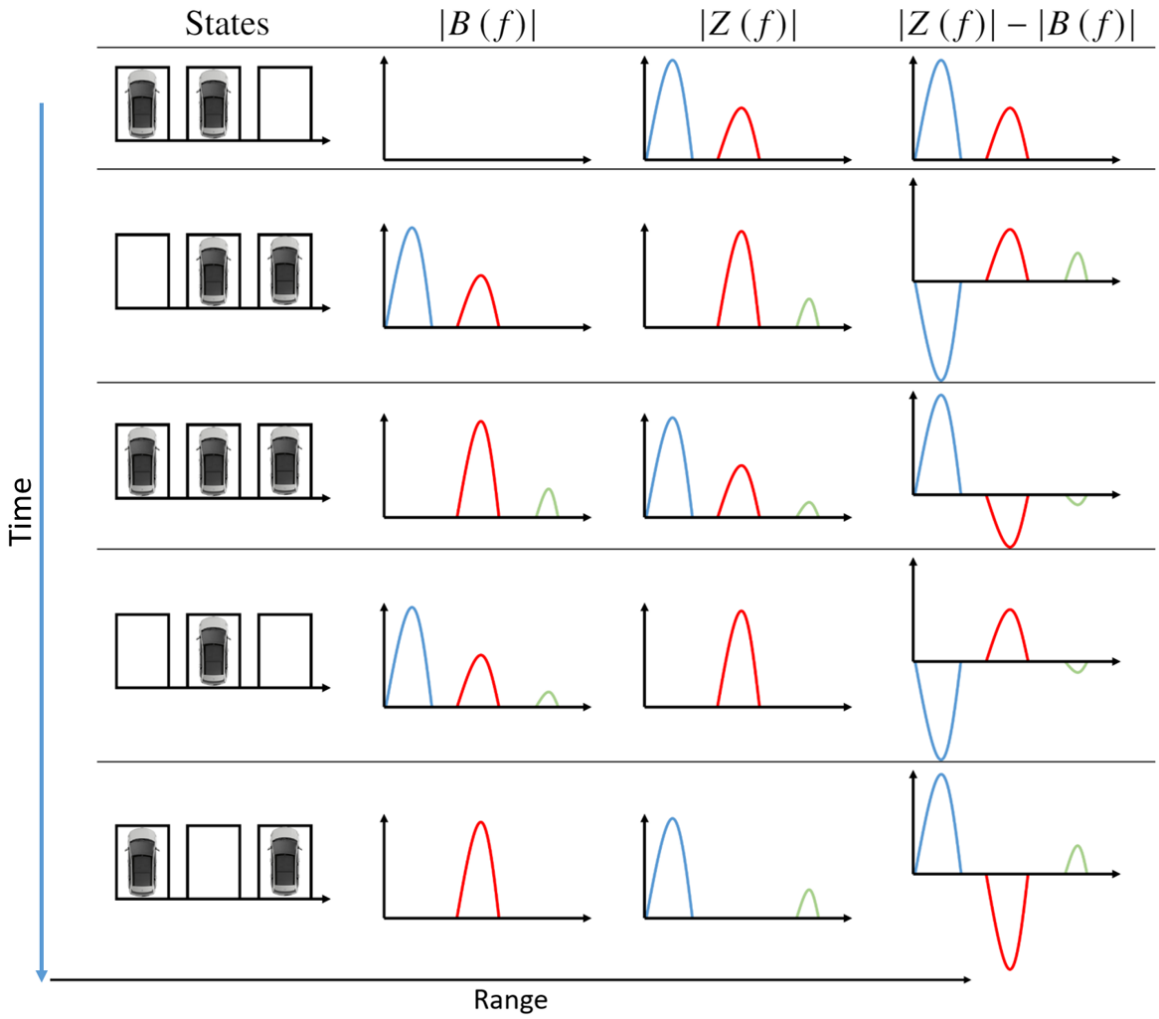

Figure 3.8: Entering or exiting cars block the radar FoV and more than one car can move at a time. In such scenario, the BS subtraction from received signal can generate more than one peak.

yields two peaks corresponding to the 2nd and 3rd parking slots. In this scenario, for the sampling points at the 1st parking slot, firstly a peak occurs in $|B(f)|$ then it disappeared in $|Z(f)|$. By subtracting background a negative peak appears in $|Z(f)| - |B(f)|$. So it represents a car is leaving. For the sampling points at the 2nd parking slot, although a positive peak occurs in $|Z(f)| - |B(f)|$, same phenomena also happens in $|B(f)|$ and $|Z(f)|$. So the car is most likely to keep stationary. Other scenarios follow the same strategy.

Because the algorithm in the third scenario is the most universal, the pseudo code

is listed in Algorithm. 1. Array subscripts start at zero. Parking slots are marked $1, 2, \cdots, N$ from near to far distance.

Algorithm 1: Anti-blocking Algorithm

Initialize Experiment Setup and Memory $M = [0, 1, 2, \cdots]$.
Initialize F_s: Sampling frequency.
c: light velocity.
T: Chirp duration time.
B: Chirp bandwidth.
N: Fast Fourier Transform (FFT) Points
Data: Determine two thresholds η_1 and η_2
Data: Initialize background data $b(k)$
while 1 **do**
  Data: Record received signal $z(k)$
  $x(k) = z(k) - b(k)$
  $B(n) = |FFT(b(k))|$
  $Z(n) = |FFT(z(k))|$
  $X(n) = |FFT(x(k))|$
  $flag = 0$. $p = 0$
  while $flag < N$ **do**
    if $|X(flag)| > \eta_1$ **then**
      $I(p) = flag$
      $p = p + 1$
    end
    $flag = flag + 1$
  end
  $p = 0$
  while $I(p) \neq NULL$ **do**
    if $X(I(p)) > 0 \&\& X(I(p))/Z(I(p)) > \eta_2$ **then**
      Compute range $R = I(p) \times F_s cT/2NB$
      Calculate the corresponding parking slot q
      print("qth parking slot is Occupied.")
    end
    if $X(I(p)) < 0 \&\& X(I(p))/Z(I(p)) < -\eta_2$ **then**
      Compute range $R = I(p) \times F_s cT/2NB$
      Calculate the corresponding parking slot q
      print("qth parking slot is Empty.")
    end
    $p = p + 1$
  end
end

3.4 System Performance Analysis

In this section, we analyze the monitoring system capacity and required height of the radar.

3.4.1 Monitoring System Capacity

To detect the presence of two adjacent cars, the difference of range between both cars from the radar should be more than the range resolution of the radar defined in (2.11). Consider the model of parking lot given in Fig. 3.9, if the height of radar is h and the width of parking slot is x, the difference between the ranges of cars in pth and $(p+1)$th parking slot can be found as

$$R_{p+1} - R_p = \sqrt{\left(p + \frac{1}{2}\right)^2 x^2 + h^2} - \sqrt{\left(p - \frac{1}{2}\right)^2 x^2 + h^2}. \tag{3.6}$$

To detect two adjacent cars the path difference between the cars $R_{p+1} - R_p \geq \Delta R$. To see how the distance between the two adjacent cars changes with respect to p, we take a numerical example from KAUST outdoor parking, where $x = 2.74$m and a radar is installed at the height of $h = 3$m. In Fig. 3.10 the range difference between two neighboring parking slots p and $p+1$ is shown. The figure shows, the range difference increases with p, and when $p = 10$, it almost saturates. If the range resolution of the radar is less than 1.8m, depending on the transmitted power, theoretically, we can detect as many cars as possible.

3.4.2 Radar Height

If a bigger vehicle, such as an SUV, is parked in front of the radar, the SUV can block the radar FoV to see smaller cars parked behind it. Fig. 3.11 shows this scenario, where the radar FoV to see the middle car is blocked. In this case, the algorithm will show this parking slot a free parking slot. For such scenarios, the radar height can

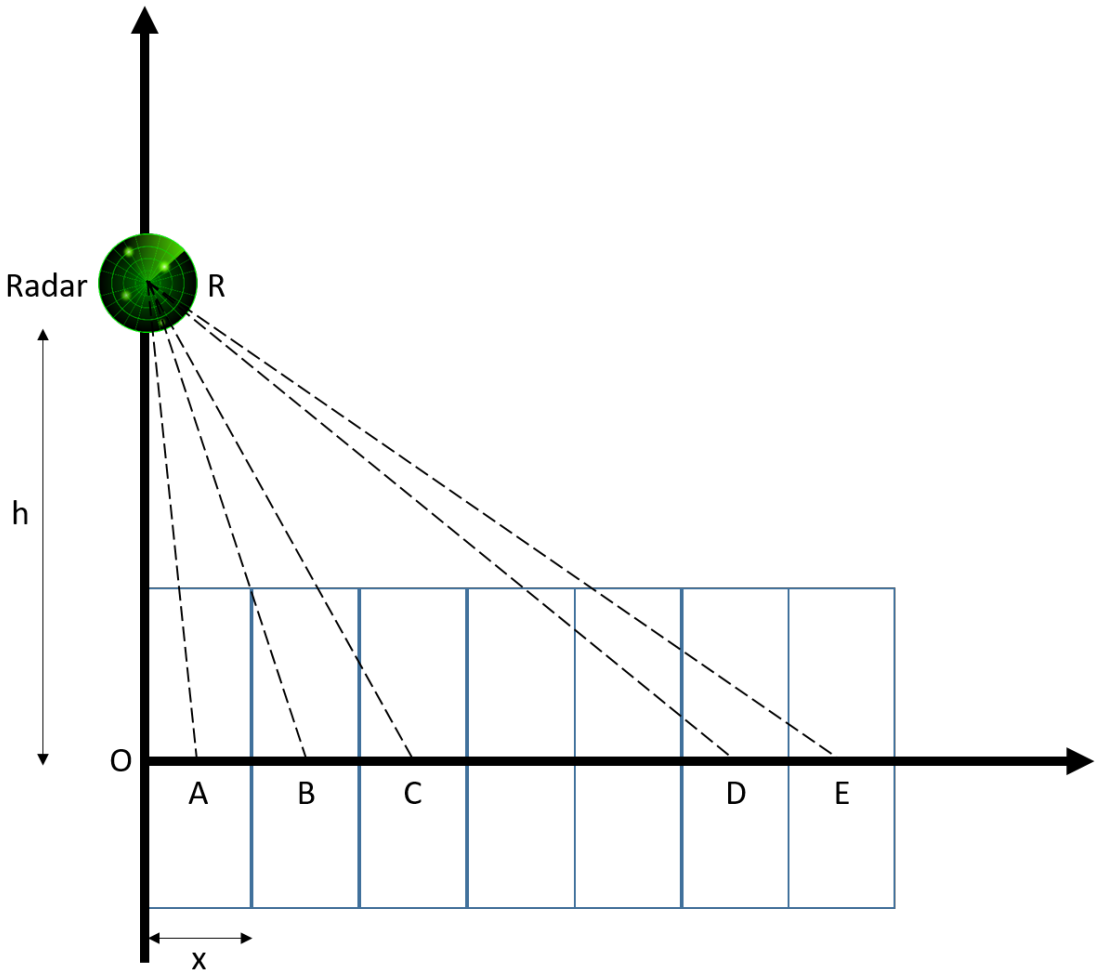

Figure 3.9: A radar is installed at height h, parking slots $A, B, \ldots, E$ are in its field of view.

be increased to see the blocked car as shown Fig. 3.12. However, increasing radar height can decrease the range difference between two cars. If the distance between two adjacent cars is less than the range resolution of the radar, it makes detection of both cars challenging. Therefore, radar FoV blockage by SUV limits the use of our proposed system.

To develop a relationship between the radar height and the height of detectable car Fig. 3.13 can be exploited. The ratio between the range to two cars is decreasing with the height of radar increasing. Suppose the height of radar is h, SUV car is h_B,

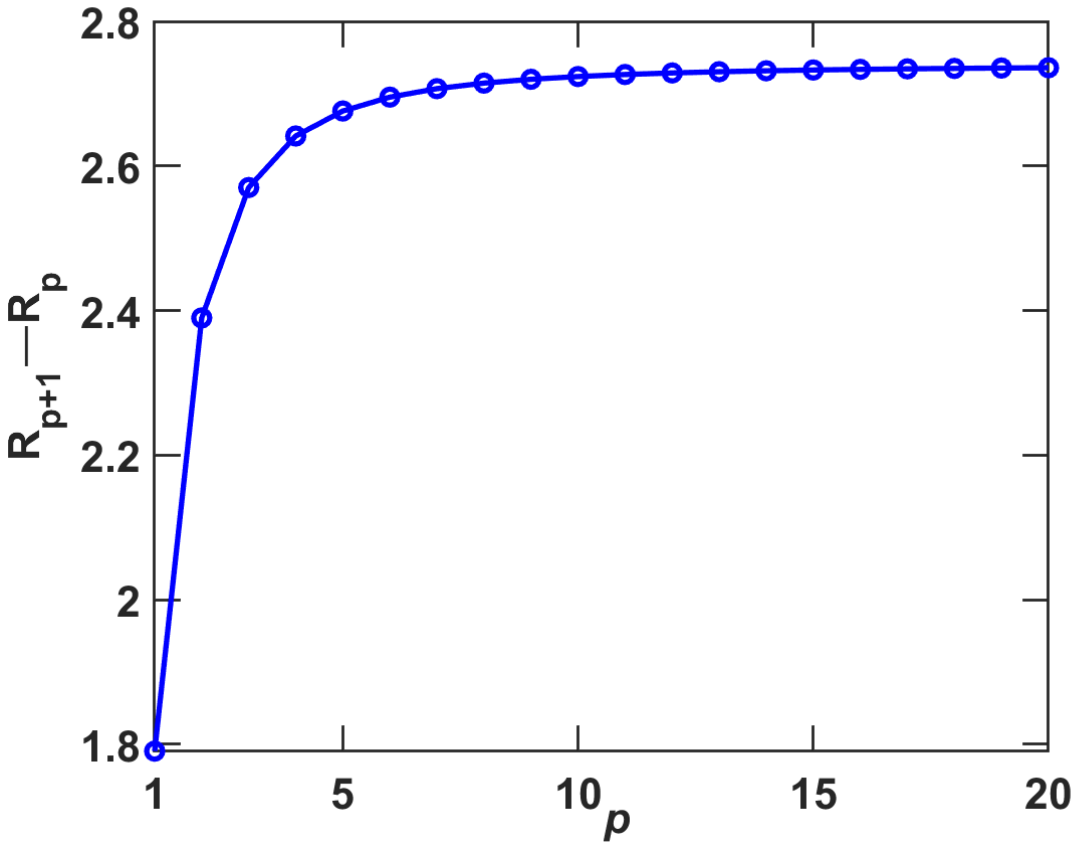

Figure 3.10: Because the range difference is increasing with N increasing, FMCW radar has infinite capacity

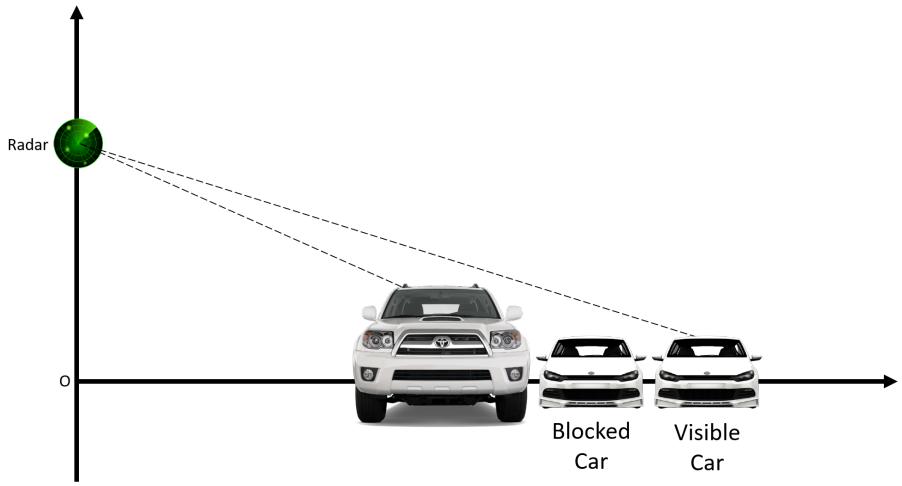

Figure 3.11: The middle smaller car is blocked by the bigger car parked in the 1st parking slot. But the car in 3rd parking slot is in the radar FoV.

and small car to be detected is h_S, then he following condition must be satisfied

$$\begin{aligned} \frac{\|RC_2\|}{\|RC_1\|} &\leq \frac{\|OB\|}{\|OA\|}, \\ \frac{\sqrt{\left(p+\frac{1}{2}\right)^2 x^2 + (h-h_S)^2}}{\sqrt{\left(p-\frac{1}{2}\right)^2 x^2 + (h-h_B)^2}} &\leq \frac{(p+\frac{1}{2})x}{(p-\frac{1}{2})x}. \end{aligned} \tag{3.7}$$

In general, the height of a Sedan car is not smaller than 1.4m and SUV is less than 2.2m. If SUV is parked in 2nd parking slot and Sedan is in 3rd Parking slot, according to (3.7), the height of the radar should be more than 3.4m.

3.5 Conclusion

In this chapter, We introduced Hamming window function to eliminate sidelobe leakage and use averaging method to suppress background noise. By taking advantage of the fact that obstacles are almost stationary, we proposed our background subtraction-based algorithm. Moving targets become more significant in the spectrum and CFAR gives us a reasonable threshold. Then we gave detail steps and block diagram for different scenarios.

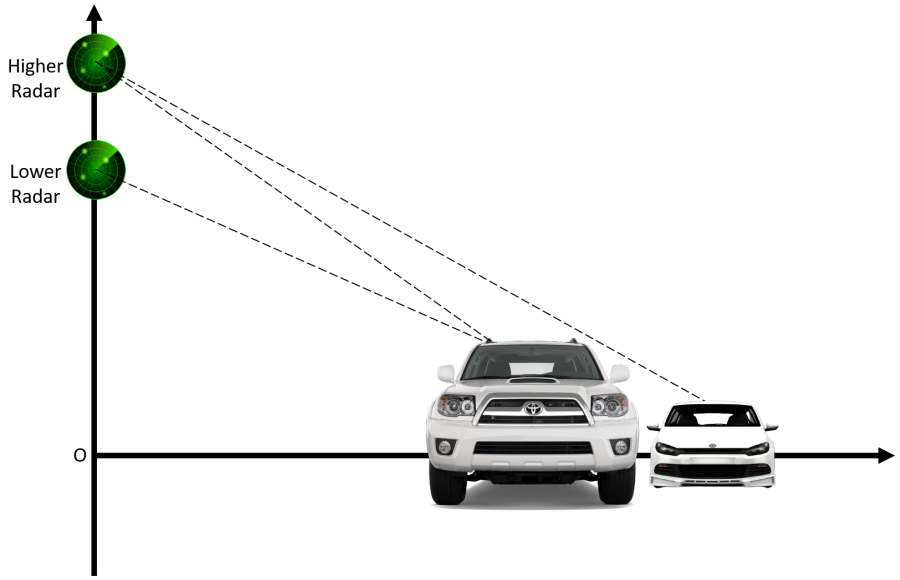

Figure 3.12: Increasing the radar height can increase the radar FoV.

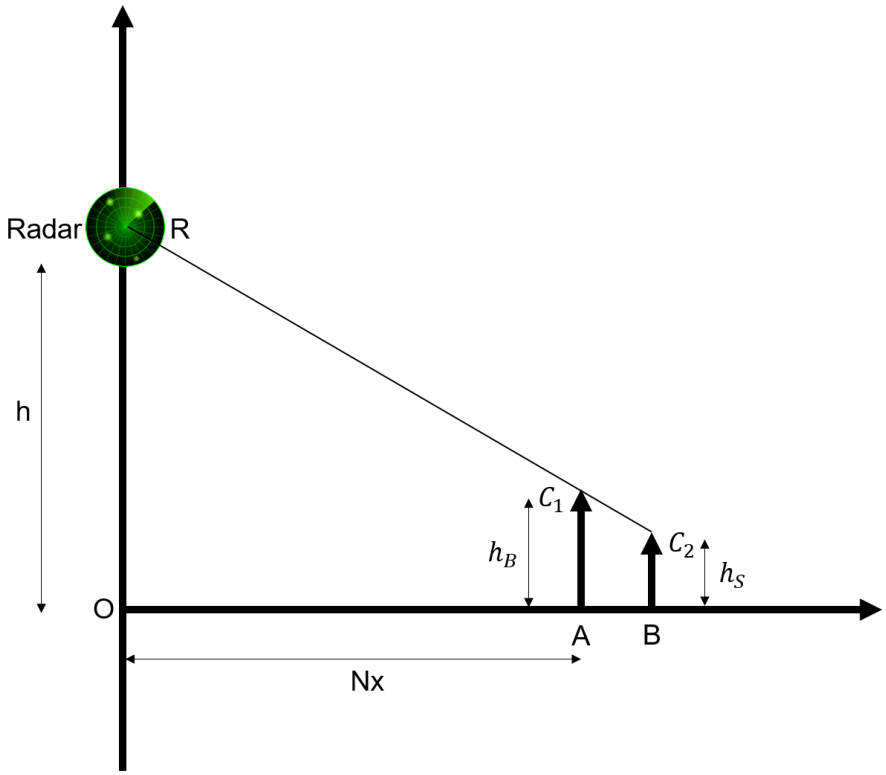

Figure 3.13: Masking influence simplification figure

Finally we analyzed the system performance and we showed that without considering power, our system will have infinite system capacity. At the same time, we put

forward a guidance for the height of radar deployment, that is, it should be higher than 3.4m.

Chapter 4

Experiment Results

In this section, we present a few screenshots of demo results. We have used the Infineon Position2Go FMCW radar module to record the demo, which has one transmit and two receive antennas. The operating frequency of the module is 24GHz, and the bandwidth is 200MHz. The duration of the chirp is set to 300μs and repeated 16 times in one frame with a frame interval of 0.2s. We monitor nine parking slots. Fig. 4.1 shows the indoor parking, seen from the radar location installed at the height of 3.0m. Fig 4.2 shows the measurement layout of the parking site, where the demo was recorded. In the layout $s_1 = 1$m, $x = 2.71$m, $s_2 = 1.3$m, and $h = 3$m. Due to some limitations in installing the radar module, the second parking slot is marked as the first parking slot in the experiment. Due to the limited availability, we have used only two cars in the experiment. The height of the first car is 1.68m, and the second is 1.47m.

The full Demo videos can be found at https://drive.google.com/drive/folders /1vsvmeVpl_C5a00Mt5JjWTkH41OU1BA0n. The demo video shows two windows. In the right- and left-hand-side windows, the synchronous scene of the parking lot and algorithm output graph are shown. In the graph, on the x-axis, the parking slot numbers are shown. After processing a data frame, the algorithm checks each parking slot to see if occupied or not. If a car is present, the algorithm assigns 1 to the corresponding memory location and draws a solid-square in the middle of the parking slot at y-axis value 1. If a car is not present in the parking slot, it assigns 0 to the corresponding memory and does not draw anything in the corresponding graph

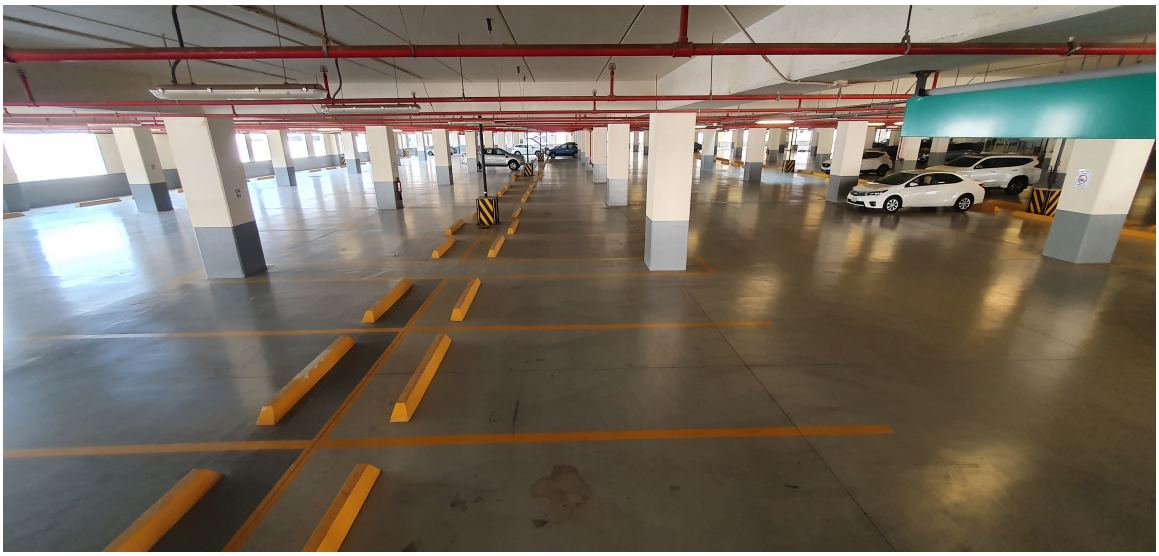

Figure 4.1: Indoor parking scene from the radar height in the radar boresight direction.

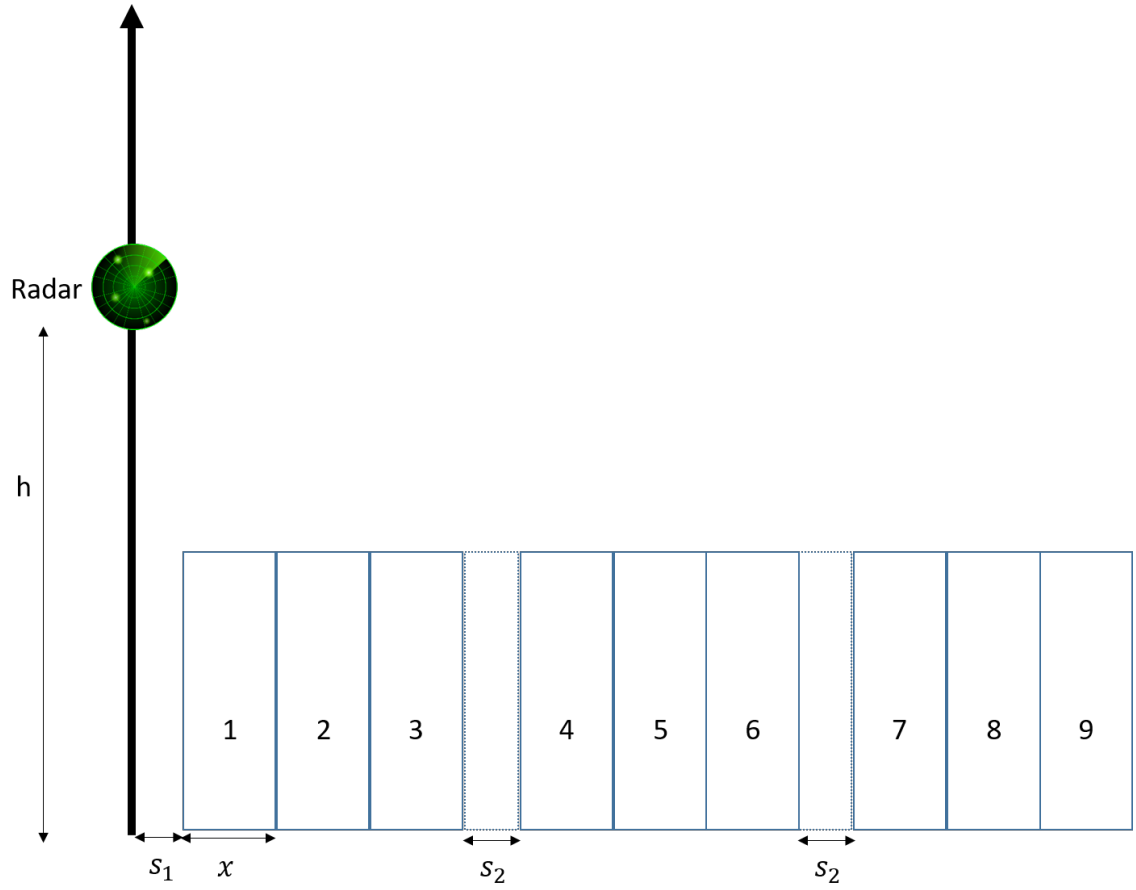

Figure 4.2: Measurement layout of the parking lot.

location. Parking Spaces are numbered from near to far from the radar. The nearest parking space is considered the first. Please note that in Fig. 4.3 to Fig. 4.6, in the surveillance picture, the index of parking slots is 1 less than the actual index. That is, we didn't take into account the actual first parking spot, because it was always occupied by a car during the study period and we couldn't move it. So it has to be treated as an obstacle. In Fig. 4.9 and Fig. 4.10 we still considered that car as an obstacle but changed the index of parking slots to make it be the same as the actual index.

The first screenshot of the demo, shown in Fig. 4.3, corresponds to the free parking lot. Here, the parking lot is free, and correspondingly the parking plot does not show any solid-square. In the second screenshot, shown in Fig. 4.4, an SUV is parked in the 1st parking slot. The algorithm processes the received signal and draws a solid square on the graph corresponding to the first parking slot as an output. In the third screenshot, shown in Fig. 4.5, 1st and 2nd parking slots are occupied by a white sedan and golden SUV. Correspondingly, the algorithm puts two solid squares in the graph. In the forth screenshot, shown in Fig. 4.6, 2nd and 3rd parking slots are occupied by a white sedan and golden SUV. Meanwhile, the result changes. The algorithm puts two solid squares on the corresponding location and the first place is shown as emptiness. In the fifth screenshot, in screenshots shown in Fig. 4.9 and Fig. 4.10, two sedans and a SUV are parked at the 2nd to the 4th parking slots. In Fig. 4.10, the SUV is more near to the radar but our system still can can detect all the three cars. So it means the blockage effect is eliminated and shows our system have good effect on detecting multiple parking slots.

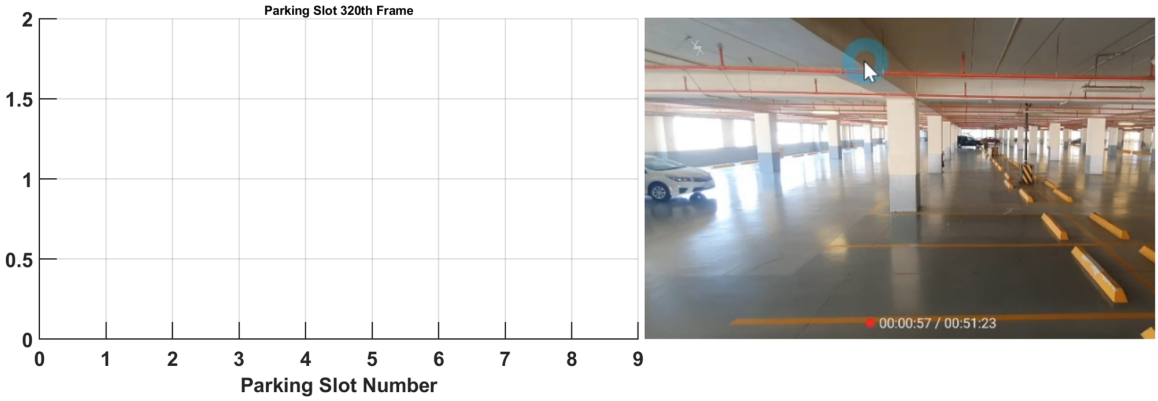

Figure 4.3: All parking slots are free.

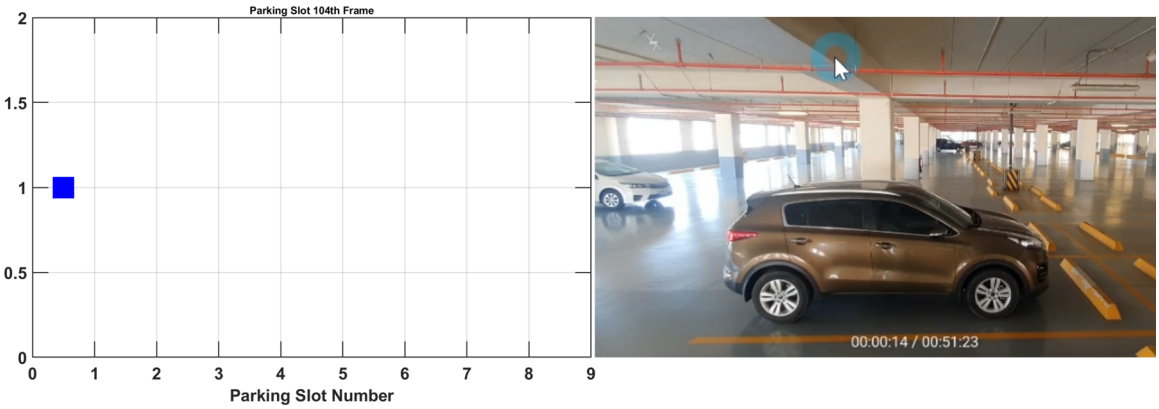

Figure 4.4: First parking slot is occupied by a golden SUV.

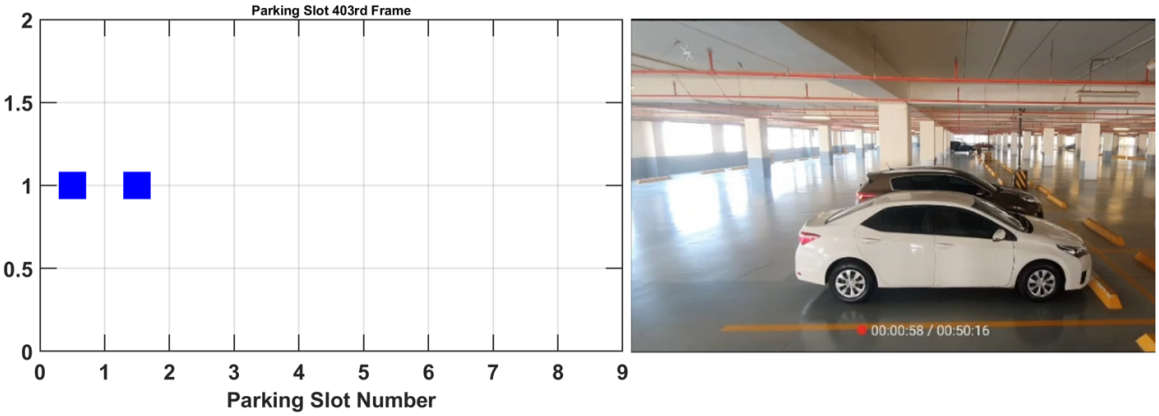

Figure 4.5: First and 2nd parking slots are respectively occupied by white sedan and golden SUV.

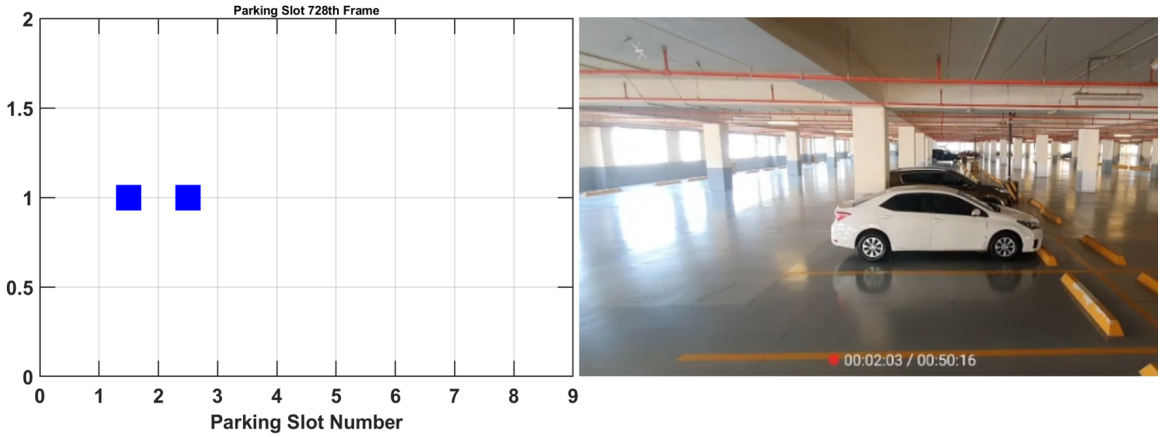

Figure 4.6: Second and 3rd parking slots are respectively occupied by white sedan and golden SUV.

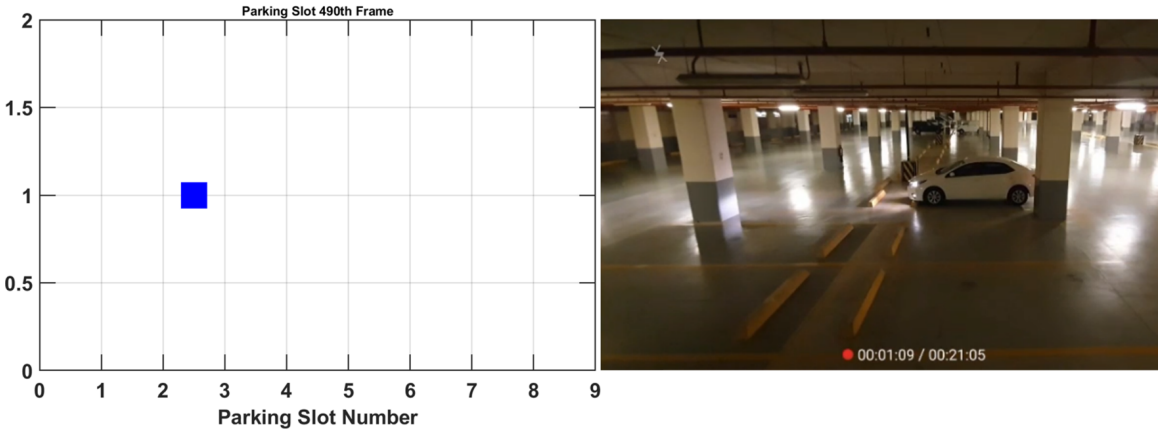

Figure 4.7: Third parking slot is occupied by white sedan.

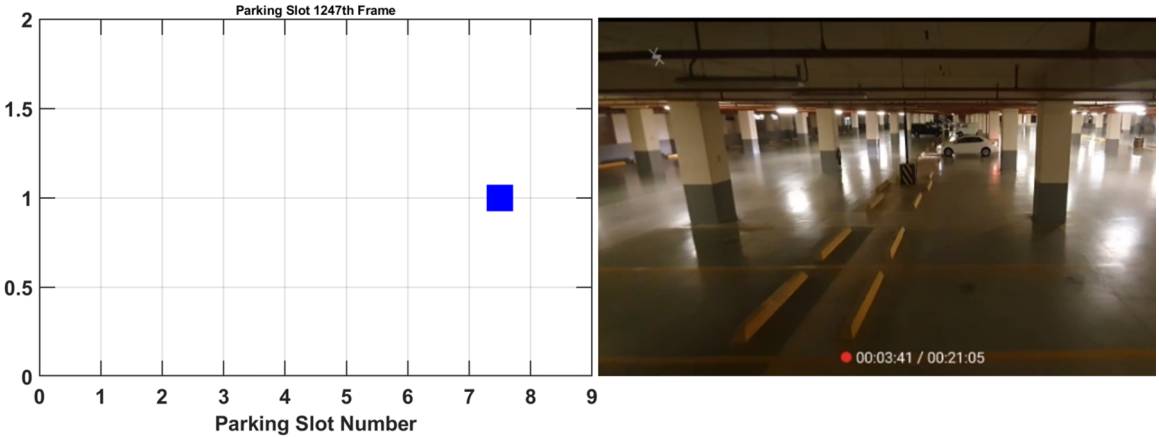

Figure 4.8: Eight parking slot is occupied by white sedan.

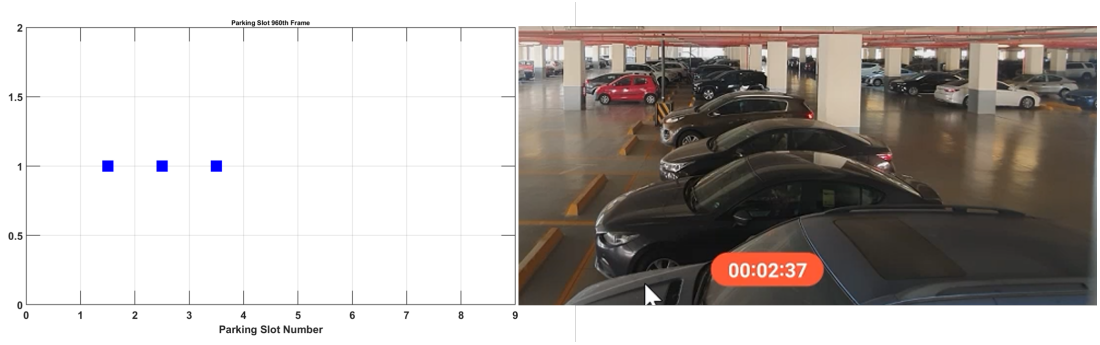

Figure 4.9: Three cars are parked from the 2nd to the 4th parking slots. Two sedans are in front of the SUV.

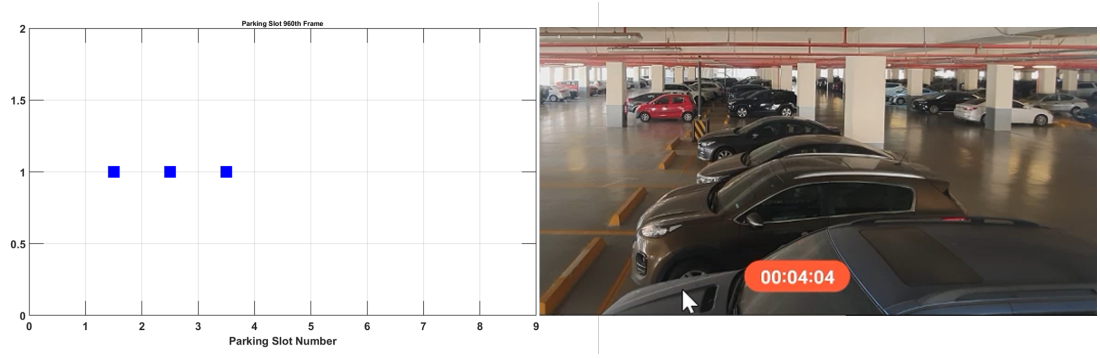

Figure 4.10: Three cars are parked from the 2nd to the 4th parking slots. The SUV is in front of two sedans. But the blockage effect has no influence.

Chapter 5

Robust target estimation algorithm

Although our system can work fine for both outdoor and indoor parking lots, it still face weak robustness and popularization difficulty. We must introduce some new theories to solve unrobust problem and increase the sensitivity of detecting targets. Estimating targets by suppressing interference and likelihood will help us to find targets accurately and reliably.

5.1 Targets' Estimation with Forward Samples

The demodulated baseband receive signal in discrete-form can be written as

$$x(n) = \alpha e^{j2\pi f_b n} + w(n), \quad n = 0, 1, \ldots, N-1, \tag{5.1}$$

where $f_b = \frac{B\tau_o}{2T} - f_d$ is the beat frequency and $\alpha = \gamma e^{j2\pi f_c \tau_o}$, and $w(n)$ is noise-plus-interference signal. To minimize the contribution of noise-plus-interference for the estimation of f_b, we split this signal into small vectors each of length M defined as

$$\begin{aligned}
\mathbf{x}(l) &= \begin{bmatrix} x(l) & x(l+1) & \cdots & x(l+M-1) \end{bmatrix}^T, \quad l = 0, 1, \ldots, N-M+1 \\
&= \alpha \begin{bmatrix} e^{j2\pi f_b l} & e^{j2\pi f_b (l+1)} & \ldots & e^{j2\pi f_b (l+M-1)} \end{bmatrix}^T + \mathbf{v}(l), \\
&= \alpha e^{j2\pi f_b l} \mathbf{a}(\omega) + \mathbf{v}(l),
\end{aligned}$$

where $\mathbf{a}(\omega) = \begin{bmatrix} 1 & e^{j2\pi f_b} & \cdots & e^{j2\pi f_b(l+M-1)} \end{bmatrix}^T$. Writing sample vectors, $\mathbf{x}(l)$s in matrix, the received signal can be written as

$$\mathbf{X} = \alpha \mathbf{A}(\omega)\mathbf{D}(\omega) + \mathbf{V}, \tag{5.2}$$

where $\mathbf{X} = \begin{bmatrix} \mathbf{x}(0) & \mathbf{x}(1) & \cdots & \mathbf{x}(N-M+1) \end{bmatrix}$, $\mathbf{A}(\omega) = \begin{bmatrix} \mathbf{a}(\omega) & \mathbf{a}(\omega) & \cdots & \mathbf{a}(\omega) \end{bmatrix}$, $\mathbf{D}(\omega) = \text{diag}\left(\mathbf{b}(\omega)\right)$ while $\mathbf{b}(\omega) = \begin{bmatrix} 1 & e^{j2\pi f} & \cdots & e^{j2\pi f(N-M+1)} \end{bmatrix}^T$. To find the value of α, the APES estimator can be found as

$$\begin{aligned} J &= \frac{1}{L}\sum_{l=0}^{L-1} \left|\mathbf{w}^H\mathbf{x}(l) - \alpha e^{j2\pi f_b l}\right|^2 + \lambda\left(\mathbf{w}^H\mathbf{a}(\omega) - 1\right), \\ &= \frac{1}{L}\sum_{l=0}^{L-1} \left(\mathbf{w}^H\mathbf{x}(l)\mathbf{x}^H(l)\mathbf{w} - \mathbf{w}^H\mathbf{x}(l)\alpha^H e^{-j2\pi f_b l} - \alpha e^{j2\pi f_b l}\mathbf{x}^H(l)\mathbf{w} + \alpha\alpha^H\right) \\ &\quad +\lambda\left(\mathbf{w}^H\mathbf{a}(\omega) - 1\right). \end{aligned} \tag{5.3}$$

The minimization of (5.3) with respect to α can be found as

$$\frac{\partial J}{\partial \alpha^*} = \frac{1}{L}\sum_{l=0}^{L-1}\left(-\mathbf{w}^H\mathbf{x}(l)e^{-j2\pi f_b l} + \alpha\right) = 0,$$

which yields

$$\hat{\alpha} = \frac{1}{L}\sum_{l=0}^{L-1}\mathbf{w}^H\mathbf{x}(l)e^{-j2\pi f_b l}.$$

Assuming $\mathbf{g}(\omega) = \frac{1}{L}\sum_{l=0}^{L-1}\mathbf{x}(l)e^{-j2\pi f_b l} = \frac{1}{L}\mathbf{X}\mathbf{b}^*(\omega)$, the estimation of α can be written in more compact form as

$$\hat{\alpha} = \mathbf{w}^H\mathbf{g}(\omega) = \frac{1}{L}\mathbf{w}^H\mathbf{X}\mathbf{b}^*(\omega), \tag{5.4}$$

where the weight vector $\mathbf{w}$ is unknown, to find its value, inserting $\hat{\alpha}$ in (5.3) the cost-function can be written as

$$J = \mathbf{w}^H \Big(\mathbf{R}_{xx} - \mathbf{g}(\omega)\mathbf{g}^H(\omega) \Big) \mathbf{w} + \lambda \left(\mathbf{w}^H \mathbf{a}(\omega) - 1 \right). \tag{5.5}$$

Assuming $\hat{\mathbf{Q}} = \big(\mathbf{R}_{xx} - \mathbf{g}(\omega)\mathbf{g}^H(\omega) \big)$, the weight vector $\mathbf{w}$ can be easily found by minimizing the cost function in (5.5) with respect to $\mathbf{w}$ as

$$\mathbf{w} = \frac{\hat{\mathbf{Q}}^{-1}\mathbf{a}(\omega)}{\mathbf{a}^H(\omega)\hat{\mathbf{Q}}^{-1}\mathbf{a}(\omega)}. \tag{5.6}$$

Inserting this value of weight vector, $\mathbf{w}$, back into (5.4) we get

$$\hat{\alpha} = \frac{1}{L} \frac{\mathbf{a}^H(\omega)\hat{\mathbf{Q}}^{-1}\mathbf{X}\mathbf{b}^*(\omega)}{\mathbf{a}^H(\omega)\hat{\mathbf{Q}}^{-1}\mathbf{a}(\omega)}. \tag{5.7}$$

In the above technique only forward samples are used to minimize the contribution of noise and interference. In the following, forward and backward samples will be used to further reduce the contribution of noise and interference.

5.2 Target's Estimation with Forward-Backward Samples

To minimize the contribution of noise and interference, for the estimation of target's range and reflection coefficient, the cost function can be written as

$$J = \frac{1}{2L} \sum_{l=0}^{L-1} \Big(\left| \mathbf{w}^H \mathbf{x}(l) - \alpha e^{j2\pi f_b l} \right|^2 + \left| \mathbf{w}^H \tilde{\mathbf{x}}(l) - \beta e^{j2\pi f_b l} \right|^2 \Big) + \lambda \left(\mathbf{w}^H \mathbf{a}(\omega) - 1 \right), \tag{5.8}$$

where $\tilde{\mathbf{x}}(l) = \begin{bmatrix} x^*(N-l-1) & x^*(N-l-2) & \cdots & x^*(N-l-M) \end{bmatrix}^T$ is a sample vector from the backward side. Assuming $\tilde{\mathbf{g}}(\omega) = \frac{1}{L} \sum_{l=0}^{L-1} \tilde{\mathbf{x}}(l) e^{-j2\pi f_b l}$ and using the same techniques used in the previous section, the minimization of the cost-function

in (5.8) with respect to α and β respectively yields

$$\hat{\alpha} = \mathbf{w}^H \mathbf{g}(\omega) = \frac{1}{L}\mathbf{w}^H \mathbf{X}\mathbf{b}^*(\omega), \tag{5.9}$$

$$\hat{\beta} = \mathbf{w}^H \tilde{\mathbf{g}}(\omega) = \frac{1}{L}\mathbf{w}^H \tilde{\mathbf{X}}\mathbf{b}^*(\omega). \tag{5.10}$$

To find $\mathbf{w}$, inserting the estimated values of α and β in the the cost-function, we get

$$\begin{aligned} J = \frac{1}{2}\left[\mathbf{w}^H \mathbf{R}_{xx}\mathbf{w} - \mathbf{w}^H \mathbf{g}(\omega)\mathbf{g}^H(\omega)\mathbf{w}\right] + \frac{1}{2}\left[\mathbf{w}^H \tilde{\mathbf{R}}_{xx}\mathbf{w} - \mathbf{w}^H \tilde{\mathbf{g}}(\omega)\tilde{\mathbf{g}}^H(\omega)\mathbf{w}\right] \\ +\lambda\left(\mathbf{w}^H \mathbf{a}(\omega) - 1\right), \\ = \mathbf{w}^H \left[\frac{1}{2}\left(\mathbf{R}_{xx} + \tilde{\mathbf{R}}_{xx}\right) - \frac{1}{2}\Big(\mathbf{g}(\omega)\mathbf{g}^H(\omega) + \tilde{\mathbf{g}}(\omega)\tilde{\mathbf{g}}^H(\omega)\Big)\right]\mathbf{w} + \lambda\left(\mathbf{w}^H \mathbf{a}(\omega) - 1\right), \end{aligned} \tag{5.11}$$

Assuming $\hat{\mathbf{Q}}_{fb} = \left[\frac{\mathbf{R}_{xx}+\tilde{\mathbf{R}}_{xx}}{2} - \frac{\mathbf{g}(\omega)\mathbf{g}^H(\omega)+\tilde{\mathbf{g}}(\omega)\tilde{\mathbf{g}}^H(\omega)}{2}\right]$, the value of $\mathbf{w}$ can be easily found by minimizing the cost-function in (5.11) with respect to $\mathbf{w}$ as

$$\mathbf{w} = \frac{\hat{\mathbf{Q}}_{fb}^{-1}\mathbf{a}(\omega)}{\mathbf{a}^H(\omega)\hat{\mathbf{Q}}_{fb}^{-1}\mathbf{a}(\omega)}. \tag{5.12}$$

Finally, inserting this value of $\mathbf{w}$ in (5.9) and (5.10), α and β can be estimated.

To show the effectiveness of forward and forward-backward samples schemes, we perform a simulation. For simulation, we assume a scenario of three targets having normalized beat frequencies 0.05, 0.1, and 0.2, and reflection coefficients' amplitudes 1, 2, and 4. The results of both schemes are compared with fast-Fourier-transform (FFT). The Fig. 5.1 and Fig. 5.2 respectively show the simulation results for $M = 10$ and $M = 20$. As can be seen in the simulations, both schemes outperform FFT to suppress side-lobe-levels (SLLs). Estimation technique with forward-backward samples in both figures suppresses interferences more efficiently compared to the forward samples only technique. It can be seen in 5.2, increasing the value of M from 10 to 20 further reduces SLLs. Moreover, with $M = 20$, the main-lobe width reduced significantly compared to $M = 10$ and simple FFT, this can improve the

range resolution of the system as well. When the amplitudes of reflection coefficients

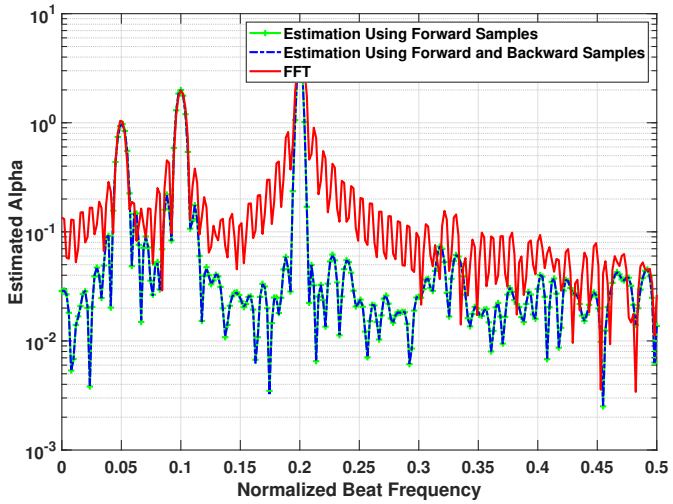

Figure 5.1: Beat frequency estimation using Forward and Forward-Backward sample vector techniques, where $N = 128$ and $M = 10$.

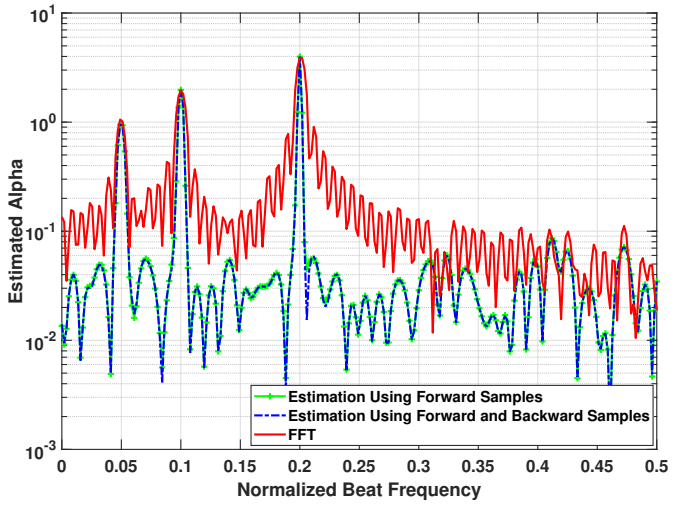

Figure 5.2: Beat frequency estimation using Forward and Forward-Backward sample vector techniques, where $N = 128$ and $M = 20$.

are much lower, the detection of targets becomes challenging using simple threshold or constant-false-alarm rate (CFAR) techniques. In such scenarios, likelihood ratio (LR) schemes can improve the detection performance significantly and independent of threshold. To find the LR of received signal, $\mathbf{X}$, in (5.2), the probability-density-

function (PDF) for given α and covariance-matrix, $\mathbf{C}$, can be written as

$$\begin{aligned} p(\mathbf{X}|\alpha,\mathbf{C}) &= \frac{1}{\pi^M|\mathbf{C}|^L}e^{-\left(\mathbf{X}-\alpha\mathbf{A}(\omega)\mathbf{D}(\omega)\right)\mathbf{C}^{-1}\left(\mathbf{X}-\alpha\mathbf{A}(\omega)\mathbf{D}(\omega)\right)^H}, \\ &= \frac{1}{\pi^M|\mathbf{C}|^L}e^{-\operatorname{Tr}\left(\mathbf{C}^{-1}(\mathbf{X}-\alpha\mathbf{A}(\omega)\mathbf{D}(\omega))^H(\mathbf{X}-\alpha\mathbf{A}(\omega)\mathbf{D}(\omega))\right)}. \end{aligned} \tag{5.13}$$

The LR can be written as

$$\mathrm{LR}(\omega) = 1 - \left(\frac{p(\mathbf{X}|\alpha=0,\mathbf{C})}{p(\mathbf{X}|\alpha,\mathbf{C})}\right)^{1/L}, \tag{5.14}$$

where the numerator of second term represent the PDF of received signal in the absence of target (also called hypothesis 0 or $\mathcal{H}_0$) while the denominator represent the PDF of received signal in the presence of target (also called hypothesis 1 or $\mathcal{H}_1$). If a target is present in the signal, $\mathrm{LR}=1$ otherwise $\mathrm{LR}=0$. Now, we will see what will be the maximum value under both hypothesises. In the absence of target, $\alpha=0$ and $\mathbf{C}=\frac{\mathbf{X}\mathbf{X}^H}{L}=\mathbf{R}_{xx}$, the PDF under hypothesis, $\mathcal{H}_0$ will give the maximum value given by

$$\begin{aligned} p(\mathbf{X}|\alpha=0,\mathbf{C}) &= \frac{1}{\pi^{LM}|\mathbf{R}_{xx}|^L}e^{-\operatorname{Tr}\left(\mathbf{R}_{xx}^{-1}\mathbf{X}^H\mathbf{X}\right)}, \\ &= \frac{1}{\pi^{LM}|\mathbf{R}_{xx}|^L}e^{-LM}. \end{aligned}$$

In the presence of unknown target, $\mathbf{C}=\frac{\left(\mathbf{X}-\alpha\mathbf{a}(\omega)\mathbf{b}^T(\omega)\right)\left(\mathbf{X}-\alpha\mathbf{a}(\omega)\mathbf{b}^T(\omega)\right)^H}{L}$, the PDF under hypothesis, $\mathcal{H}_1$ can be calculated using (5.13) as

$$p(\mathbf{X}|\alpha,\mathbf{C}) = \frac{1}{\pi^{LM}|\mathbf{C}|^L}e^{-LM}$$

To maximise $p(\mathbf{X}|\alpha,\mathbf{C})$, the determinant $|\mathbf{C}|$ should be minimum with respect to α.

Therefore,

$$\begin{aligned}
|\mathbf{C}| &= \left|\frac{1}{L}\Big(\left(\mathbf{X} - \alpha\mathbf{a}(\omega)\mathbf{b}^T(\omega)\right)\left(\mathbf{X} - \alpha\mathbf{a}(\omega)\mathbf{b}^T(\omega)\right)^H \Big)\right|, \\
&= \left|\frac{1}{L}\Big(\mathbf{X}\mathbf{X}^H - \mathbf{X}\mathbf{b}^*(\omega)\mathbf{a}^H(\omega)\alpha^* - \alpha\mathbf{a}(\omega)\mathbf{b}^T(\omega)\mathbf{X}^H + \alpha\mathbf{a}(\omega)\mathbf{b}^T(\omega)\mathbf{b}^*(\omega)\mathbf{a}^H(\omega)\alpha^*\Big)\right|.
\end{aligned}$$

Using $\hat{\mathbf{Q}} = \left(\mathbf{R}_{xx} - \mathbf{g}(\omega)\mathbf{g}^H(\omega)\right)$ from the previous section, we can write

$$\begin{aligned}
|\mathbf{C}| &= \left|\hat{\mathbf{Q}} + \mathbf{g}(\omega)\mathbf{g}^H(\omega) + \frac{1}{L}\Big(- \mathbf{X}\mathbf{b}^*(\omega)\mathbf{a}^H(\omega)\alpha^* - \alpha\mathbf{a}(\omega)\mathbf{b}^T(\omega)\mathbf{X}^H + \alpha\mathbf{a}(\omega)L\mathbf{a}^H(\omega)\alpha^*\Big)\right|, \\
&= \left|\hat{\mathbf{Q}} + \frac{1}{L^2}\mathbf{X}\mathbf{b}^*(\omega)\mathbf{b}^T(\omega)\mathbf{X}^H - \frac{1}{L}\Big(\mathbf{X}\mathbf{b}^*(\omega)\mathbf{a}^H(\omega)\alpha^* + \alpha\mathbf{a}(\omega)\mathbf{b}^T(\omega)\mathbf{X}^H - \alpha\mathbf{a}(\omega)L\mathbf{a}^H(\omega)\alpha^*\Big)\right|, \\
&= \left|\hat{\mathbf{Q}} + \left(\alpha\mathbf{a}(\omega) - \frac{\mathbf{X}\mathbf{b}^*(\omega)}{L}\right)\left(\alpha\mathbf{a}(\omega) - \frac{\mathbf{X}\mathbf{b}^*(\omega)}{L}\right)^H\right|, \\
&= \left|\hat{\mathbf{Q}}\left(\mathbf{I} + \hat{\mathbf{Q}}^{-1}\left(\alpha\mathbf{a}(\omega) - \frac{\mathbf{X}\mathbf{b}^*(\omega)}{L}\right)\left(\alpha\mathbf{a}(\omega) - \frac{\mathbf{X}\mathbf{b}^*(\omega)}{L}\right)^H\right)\right|. \qquad (5.15)
\end{aligned}$$

Using the determinant identity $|\mathbf{I} + \mathbf{A}\mathbf{B}| = |\mathbf{I} + \mathbf{B}\mathbf{A}|$, the determinant in (5.15) can be written in simple form as

$$|\mathbf{C}| = \left|\hat{\mathbf{Q}}\right|\left(1 + \left(\alpha\mathbf{a}(\omega) - \frac{\mathbf{X}\mathbf{b}^*(\omega)}{L}\right)^H \hat{\mathbf{Q}}^{-1}\left(\alpha\mathbf{a}(\omega) - \frac{\mathbf{X}\mathbf{b}^*(\omega)}{L}\right)\right).$$

Here, if we use the estimated value of α from (5.7), we can say

$$|\mathbf{C}| \geq \left|\hat{\mathbf{Q}}\right|\left(1 + \psi_1\hat{\mathbf{Q}}^{-1}\psi_1^H\right)$$

where

$$\psi_1 = \left(\frac{1}{L}\frac{\mathbf{a}^H(\omega)\hat{\mathbf{Q}}^{-1}\mathbf{X}\mathbf{b}^*(\omega)}{\mathbf{a}^H(\omega)\hat{\mathbf{Q}}^{-1}\mathbf{a}(\omega)}\mathbf{a}(\omega) - \frac{\mathbf{X}\mathbf{b}^*(\omega)}{L}\right)^H$$

Determine

$$\begin{aligned} \xi_1 &= \frac{1}{L^2}\mathbf{b}^T(\omega)\mathbf{X}^H\left(\frac{\hat{\mathbf{Q}}^{-1}\mathbf{a}(\omega)}{\mathbf{a}^H(\omega)\hat{\mathbf{Q}}^{-1}\mathbf{a}(\omega)}\mathbf{a}^H(\omega)-\mathbf{I}\right) \\ \xi_2 &= \left(\mathbf{a}(\omega)\frac{\mathbf{a}^H(\omega)\hat{\mathbf{Q}}^{-1}}{\mathbf{a}^H(\omega)\hat{\mathbf{Q}}^{-1}\mathbf{a}(\omega)}-\mathbf{I}\right) \end{aligned} \tag{5.16}$$

Therefore, the minimum value of $|\mathbf{C}|$ will be

$$\begin{aligned} |\mathbf{C}|_{\min} &= \left|\hat{\mathbf{Q}}\right|\left(1+\xi_1\hat{\mathbf{Q}}^{-1}\xi_2\mathbf{X}\mathbf{b}^*(\omega)\right), \\ &= \left|\hat{\mathbf{Q}}\right|\left(1-\frac{1}{L^2}\mathbf{b}^T(\omega)\mathbf{X}^H\left(\frac{\hat{\mathbf{Q}}^{-1}\mathbf{a}(\omega)\mathbf{a}^H(\omega)\hat{\mathbf{Q}}^{-1}}{\mathbf{a}^H(\omega)\hat{\mathbf{Q}}^{-1}\mathbf{a}(\omega)}+\hat{\mathbf{Q}}^{-1}\right)\mathbf{X}\mathbf{b}^*(\omega)\right), \\ &= \left|\hat{\mathbf{Q}}\right|\left|\mathbf{I}-\left(\frac{\hat{\mathbf{Q}}^{-1}\mathbf{a}(\omega)\mathbf{a}^H(\omega)\hat{\mathbf{Q}}^{-1}}{\mathbf{a}^H(\omega)\hat{\mathbf{Q}}^{-1}\mathbf{a}(\omega)}-\hat{\mathbf{Q}}^{-1}\right)\mathbf{X}\mathbf{b}^*(\omega)\frac{1}{L^2}\mathbf{b}^T(\omega)\mathbf{X}^H\right|. \end{aligned}$$

In the last step, we have again used the identity $|\mathbf{I}+\mathbf{AB}|=|\mathbf{I}+\mathbf{BA}|$. Now using the identity, $|\mathbf{A}||\mathbf{B}|=|\mathbf{AB}|$, we can write

$$|\mathbf{C}|_{\min} = \left|\hat{\mathbf{Q}}+\frac{1}{L^2}\left(\mathbf{I}-\frac{\mathbf{a}(\omega)\mathbf{a}^H(\omega)\hat{\mathbf{Q}}^{-1}}{\mathbf{a}^H(\omega)\hat{\mathbf{Q}}^{-1}\mathbf{a}(\omega)}\right)\mathbf{X}\mathbf{b}^*(\omega)\mathbf{b}^T(\omega)\mathbf{X}^H\right|.$$

It can be easily prove that $\mathbf{g}(\omega)=\frac{1}{L}\mathbf{X}\mathbf{b}^*(\omega)$, therefore $\hat{\mathbf{Q}}=\left(\mathbf{R}_{xx}-\mathbf{g}(\omega)\mathbf{g}^H(\omega)\right)$ can also be written as $\hat{\mathbf{Q}}=\left(\mathbf{R}_{xx}-\frac{1}{L^2}\mathbf{X}\mathbf{b}^*(\omega)\mathbf{b}^T(\omega)\mathbf{X}^H\right)$, and we can write

$$\begin{aligned} |\mathbf{C}|_{\min} &= \left|\hat{\mathbf{R}}_{xx}-\frac{\mathbf{X}\mathbf{b}^*(\omega)\mathbf{b}^T(\omega)\mathbf{X}^H}{L^2}+\frac{1}{L^2}\left(\mathbf{I}-\frac{\mathbf{a}(\omega)\mathbf{a}^H(\omega)\hat{\mathbf{Q}}^{-1}}{\mathbf{a}^H(\omega)\hat{\mathbf{Q}}^{-1}\mathbf{a}(\omega)}\right)\mathbf{X}\mathbf{b}^*(\omega)\mathbf{b}^T(\omega)\mathbf{X}^H\right|, \\ &= \left|\hat{\mathbf{R}}_{xx}-\frac{\mathbf{a}(\omega)\mathbf{a}^H(\omega)\hat{\mathbf{Q}}^{-1}\mathbf{X}\mathbf{b}^*(\omega)\mathbf{b}^T(\omega)\mathbf{X}^H}{L^2\mathbf{a}^H(\omega)\hat{\mathbf{Q}}^{-1}\mathbf{a}(\omega)}\right|, \\ &= \left|\hat{\mathbf{R}}_{xx}-\frac{\mathbf{a}(\omega)\mathbf{a}^H(\omega)\hat{\mathbf{Q}}^{-1}}{\mathbf{a}^H(\omega)\hat{\mathbf{Q}}^{-1}\mathbf{a}(\omega)}\left(\hat{\mathbf{R}}_{xx}-\hat{\mathbf{Q}}\right)\right|. \end{aligned}$$

Using the identity $|\mathbf{A}||\mathbf{B}| = |\mathbf{AB}|$ and $|\mathbf{I} + \mathbf{AB}| = |\mathbf{I} + \mathbf{BA}|$, we can further simplify

$$\begin{aligned}
|\mathbf{C}|_{\min} &= \left|\hat{\mathbf{R}}_{xx}\right| \left|\mathbf{I} - \frac{\hat{\mathbf{R}}_{xx}^{-1}\mathbf{a}(\omega)\mathbf{a}^H(\omega)\hat{\mathbf{Q}}^{-1}}{\mathbf{a}^H(\omega)\hat{\mathbf{Q}}^{-1}\mathbf{a}(\omega)}\left(\hat{\mathbf{R}}_{xx} - \hat{\mathbf{Q}}\right)\right|, \\
&= \left|\hat{\mathbf{R}}_{xx}\right| \left(1 - \mathbf{a}^H(\omega)\hat{\mathbf{Q}}^{-1}\left(\hat{\mathbf{R}}_{xx} - \hat{\mathbf{Q}}\right)\frac{\hat{\mathbf{R}}_{xx}^{-1}\mathbf{a}(\omega)}{\mathbf{a}^H(\omega)\hat{\mathbf{Q}}^{-1}\mathbf{a}(\omega)}\right), \\
&= \left|\hat{\mathbf{R}}_{xx}\right| \left|1 - \mathbf{a}^H(\omega)\left(\hat{\mathbf{Q}}^{-1}\hat{\mathbf{R}}_{xx} - \mathbf{I}\right)\frac{\hat{\mathbf{R}}_{xx}^{-1}\mathbf{a}(\omega)}{\mathbf{a}^H(\omega)\hat{\mathbf{Q}}^{-1}\mathbf{a}(\omega)}\right|, \\
&= \left|\hat{\mathbf{R}}_{xx}\right| \left(1 - \mathbf{a}^H(\omega)\left(\hat{\mathbf{Q}}^{-1} - \hat{\mathbf{R}}_{xx}^{-1}\right)\frac{\mathbf{a}(\omega)}{\mathbf{a}^H(\omega)\hat{\mathbf{Q}}^{-1}\mathbf{a}(\omega)}\right), \\
&= \left|\hat{\mathbf{R}}_{xx}\right| \left(\frac{\mathbf{a}^H(\omega)\hat{\mathbf{R}}_{xx}^{-1}\mathbf{a}(\omega)}{\mathbf{a}^H(\omega)\hat{\mathbf{Q}}^{-1}\mathbf{a}(\omega)}\right).
\end{aligned}$$

Therefore, the LR in (5.14) can be written as

$$\begin{aligned}
\mathrm{LR}(\omega) &= 1 - \left(\frac{\frac{1}{\pi^{LM}|\mathbf{R}_{xx}|^L}e^{-LM}}{\frac{1}{\pi^{LM}|\mathbf{C}|^L}e^{-LM}}\right)^{1/L} \\
&= 1 - \left(\frac{\mathbf{a}^H(\omega)\hat{\mathbf{R}}_{xx}^{-1}\mathbf{a}(\omega)}{\mathbf{a}^H(\omega)\hat{\mathbf{Q}}^{-1}\mathbf{a}(\omega)}\right)
\end{aligned}$$

Using the same strategy used for forward samples, the LR using forward and backward samples can be written as

$$\mathrm{LR}(\omega) = 1 - \frac{\mathbf{a}^H(\omega)\left(\frac{\hat{\mathbf{R}}_{xx}+\tilde{\mathbf{R}}_{xx}}{2}\right)^{-1}\mathbf{a}(\omega)}{\mathbf{a}^H(\omega)\hat{\mathbf{Q}}_{fb}^{-1}\mathbf{a}(\omega)}$$

To see the performance of the LR with forward and forward-backward samples, we perform two simulation with $M = 10$ and $M = 20$. We use the previous scenario of three targets at $f_b = 0.05$, $f_b = 0.1$, and $f_b = 0.2$. The corresponding simulation results are shown in Fig. 5.3 and Fig. 5.4. It can be seen in the figures in both simulation the target with likelihood ratio of almost equal to one can be identified. The advantage of using forward-backward sample technique is the lower values of LRs

at the locations where target is not present. It should also be noted that increasing the value of $M = 10$ to $M = 20$ have no gain rather LRs at locations where target is not present has increased.

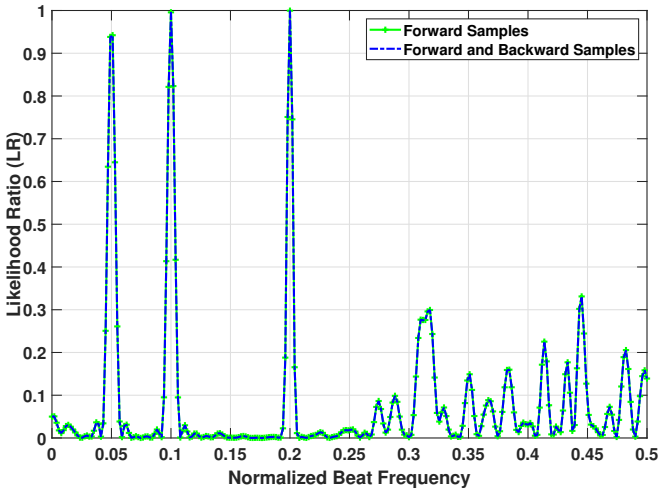

Figure 5.3: Target estimation using LR with Forward and Forward-Backward sample vector techniques, where $N = 128$ and $M = 10$.

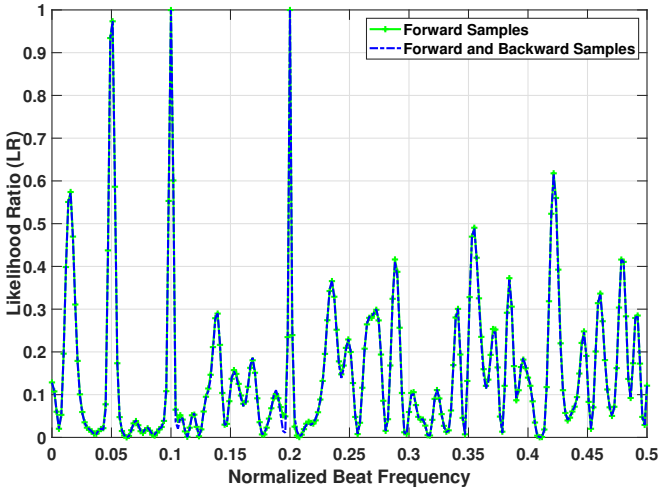

Figure 5.4: Target estimation using LR with Forward and Forward-Backward sample vector techniques, where $N = 128$ and $M = 20$.

Chapter 6

Future work

To promote our system, we plan to connect our system with Internet and develop an APP. So parking managers only need to deploy our system once and guide drivers to download our APP. Then drivers can master the information of all parking slots all the time.

In our proposed solution, once the parking slots occupancy (PSO) is known, it is made available online through a mobile and web application. Fig. 6.1 shows the flow of PSO data from the Position2Go module to the mobile and web application. First, we use the position2Go module's serial port to send raw/processed data to the external world. Therefore, the serial port is interfaced with the ESP32/ESP8266 WiFi module to read the PSO data from the Position2Go module. All processing is performed in the Position2Go module in the current system, and data is transferred to the WiFi module in text format. We use the MQ telemetry transport (MQTT) protocol to make the data available for mobile and web applications from the WiFi module. The developed mobile app and website allow users to see the free/occupied parking slots and book them. To use this application, the vehicle user must have internet access.

For offline users, at the parking entrance, each vehicle is allocated a parking slot. The vehicle user is bound to park in his allocated slot. Whenever a parking slot is freed or occupied, the algorithm updates parking slot memory. The above software can be used independently, where it can receive the PSO data from sensors other than radar such as camera and infra-red. To show reserved parking, a predefined

color light in the free parking slot can represent an already booked parking slot.

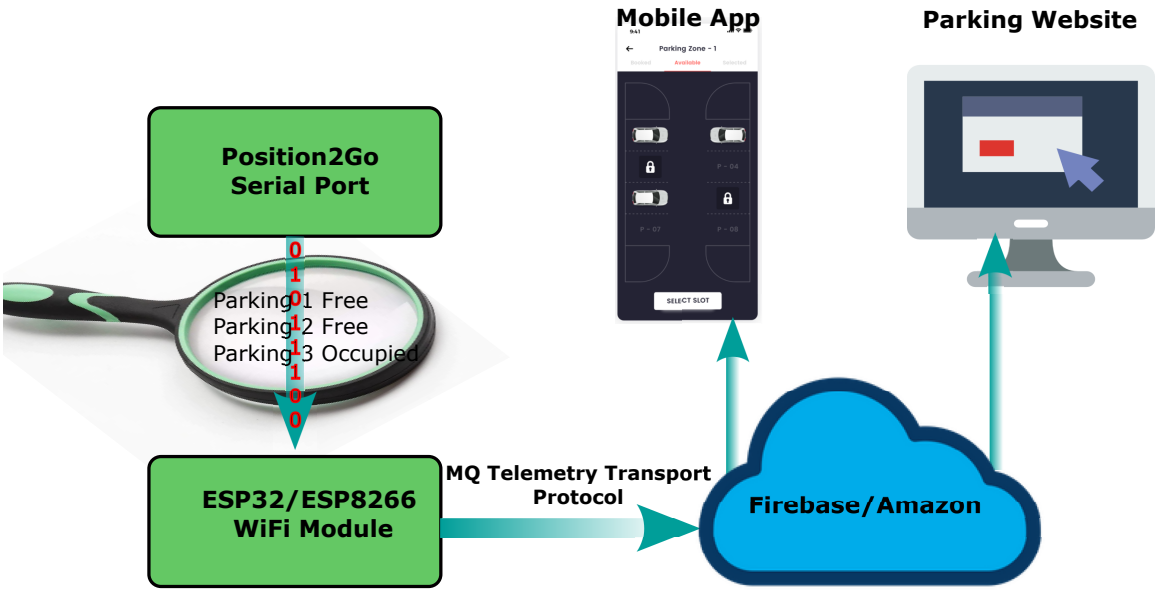

Figure 6.1: The flow of parking occupancy data from Position2Go module to Mobile and web applications.

Chapter 7

Conclusion

In this thesis, the main work can be summarized as follows.

In Chapter 2, we first discussed the importance and broad usage of FMCW radar and CFAR. Then the FMCW radar signal is modelled and we derived closed expression of target range with respect to the radar parameters. So the feasibility of using FMCW radar to monitor parking lots is clear. In the next step, we showed the steps of CFAR and gave an example. Finally we showed some experiment results and explained how we can distinguish cars with the help of radar and CFAR. This chapter focused most on feasibility and fundamental theory.

In Chapter 3, we explained main challenges we faced in experiment. For background noise we adopted averaging method and Hamming window function is used for suppressing sidelobe leakage. However, they cannot help us eliminating environment obstacles such as pillars and pipes in the parking lots. Then we proposed our background-subtraction-based algorithm. By calculating the difference of two frames the moving targets become more clear so we can distinguish cars from several strong signal. Next, we gave detail steps and corresponding block diagrams for three different scenarios. Finally system performance analysis shows our system can have theoretically infinite capacity. The height of radar should be taller than 3.4m for the best result. This chapter mainly focus on algorithm details such as diagram and pseudo codes.

In Chapter 4 we showed experiment results and demo videos. Through field experiments, our system can reflect the parking situation in real time and give accurate

results quickly. Our system can observe multiple parking Spaces at the same time and effectively eliminate the blocking effect of large cars on small cars. At the same time, the furthest observation distance can reach more than 30 meters. In addition, small size and low power consumption are also advantages of our system.

In Chapter 5 we talked about future work. One potential work is weak robustness. we introduced the theory on target estimation by suppressing interference and likelihood. By further suppressing clutter and hypothesis - test methods, we hope to further improve the robustness and sensitivity of our system. The other potential work is improving user experience in our system. We are trying to connect the radar with WiFi modulo then with Internet to share the information of parking lots online. Therefore, drivers can be informed of the parking lots information all the time without having to go there in person. This enhances user friendliness and reduces the work load of parking managers.

REFERENCES

[1] L. Gan, "Globalization of the automobile industry in china: dynamics and barriers in greening of the road transportation," *Energy policy*, vol. 31, no. 6, pp. 537–551, 2003.

[2] X. Deng, "Private car ownership in china: How important is the effect of income?" Ph.D. dissertation, Citeseer, 2007.

[3] A. Zajam and S. Dholay, "Detecting efficient parking space using smart parking," in *2018 9th International Conference on Computing, Communication and Networking Technologies (ICCCNT)*. IEEE, 2018, pp. 1–7.

[4] A. Loeffler, J. Ronczka, and T. Fechner, "Parking lot measurement with 24 ghz short range automotive radar," in *2015 16th International Radar Symposium (IRS)*. IEEE, 2015, pp. 137–142.

[5] R. Prophet, M. Hoffmann, M. Vossiek, G. Li, and C. Sturm, "Parking space detection from a radar based target list," in *2017 IEEE MTT-S International Conference on Microwaves for Intelligent Mobility (ICMIM)*. IEEE, 2017, pp. 91–94.

[6] M. S. Al-Ani and Z. A. Kakarash, "Future aspects of intelligent car parking based on internet of things," *UHD journal of science and technology*, vol. 2, no. 1, pp. 19–26, 2018.

[7] M. Swaraj, M. K. Munagala, P. Bharti, and C. Jayavarthini, "smart parking system using facial recognition, optical character recognition and internet of things (iot)," *Int. Res. J. Eng. Technol*, vol. 6, pp. 1278–1282, 2019.

[8] A. Athira, S. Lekshmi, P. Vijayan, and B. Kurian, "Smart parking system based on optical character recognition," in *2019 3rd International Conference on Trends in Electronics and Informatics (ICOEI)*. IEEE, 2019, pp. 1184–1188.

[9] J. Martinez Garcia, "Classification of mimo-fmcw radar images with convolutional neural networks in a parking monitoring application," Ph.D. dissertation, Friedrich-Alexander-Universität Erlangen-Nürnberg (FAU), 2020.

[10] L. Brown, *Technical and military imperatives: a radar history of World War 2*. Crc Press, 1999.

[11] F. Bekkadal, "Novel radar technology and applications," in *17th International Conference on Applied Electromagnetics and Communications, 2003. ICECom 2003.* IEEE, 2003, pp. 6–12.

[12] R. C. Harney, "Military applications of coherent infrared radar," in *Physics and Technology of Coherent Infrared Radar I*, vol. 300. International Society for Optics and Photonics, 1982, pp. 2–11.

[13] J. D. Taylor, *Ultra-wideband radar technology.* CRC press, 2000.

[14] D. Daniels, "Applications of impulse radar technology," in *Radar 97 (Conf. Publ. No. 449).* IET, 1997, pp. 667–672.

[15] A. G. Westra, "Radar versus stealth: Passive radar and the future of us military power," NATIONAL DEFENSE UNIV WASHINGTON DC INST FOR NATIONAL STRATEGIC STUDIES, Tech. Rep., 2009.

[16] G. Rao and S. Mahulikar, "Integrated review of stealth technology and its role in airpower," *The aeronautical journal*, vol. 106, no. 1066, pp. 629–642, 2002.

[17] B. Zohuri, *Radar energy warfare and the challenges of stealth technology.* Springer, 2020.

[18] J. Pinto, J. Matthews, and C. Sarno, "Radar signature reduction of wind turbines through the application of stealth technology," in *2009 3rd European Conference on Antennas and Propagation.* IEEE, 2009, pp. 3886–3890.

[19] D. A. Ausherman, A. Kozma, J. L. Walker, H. M. Jones, and E. C. Poggio, "Developments in radar imaging," *IEEE Transactions on Aerospace and Electronic Systems*, no. 4, pp. 363–400, 1984.

[20] P. Nkwari, S. Sinha, and H. Ferreira, "Through-the-wall radar imaging: A review," *IETE technical review*, vol. 35, no. 6, pp. 631–639, 2018.

[21] A. Al-Naji, A. J. Al-Askery, S. K. Gharghan, and J. Chahl, "A system for monitoring breathing activity using an ultrasonic radar detection with low power consumption," *Journal of Sensor and Actuator Networks*, vol. 8, no. 2, p. 32, 2019.

[22] T. Zhou, M. Yang, K. Jiang, H. Wong, and D. Yang, "Mmw radar-based technologies in autonomous driving: A review," *Sensors*, vol. 20, no. 24, p. 7283, 2020.

[23] S. Sun, A. P. Petropulu, and H. V. Poor, "Mimo radar for advanced driver-assistance systems and autonomous driving: Advantages and challenges," *IEEE Signal Processing Magazine*, vol. 37, no. 4, pp. 98–117, 2020.

[24] B. Möhring, C. Moroder, U. Siart, and T. Eibert, "Broadband, fast, and linear chirp generation based on dds for fmcw radar applications," in *2019 IEEE Radar Conference (RadarConf)*. IEEE, 2019, pp. 1–4.

[25] M. Alizadeh, H. Abedi, and G. Shaker, "Low-cost low-power in-vehicle occupant detection with mm-wave fmcw radar," in *2019 IEEE SENSORS*. IEEE, 2019, pp. 1–4.

[26] J. T. Wixted, "The forgotten history of signal detection theory." *Journal of experimental psychology: learning, memory, and cognition*, vol. 46, no. 2, p. 201, 2020.

[27] C.-I. Chang, "Statistical detection theory approach to hyperspectral image classification," *IEEE Transactions on Geoscience and Remote Sensing*, vol. 57, no. 4, pp. 2057–2074, 2018.

[28] ——, "Hyperspectral target detection: Hypothesis testing, signal-to-noise ratio, and spectral angle theories," *IEEE Transactions on Geoscience and Remote Sensing*, vol. 60, pp. 1–23, 2021.

[29] L. Ye and S. Sundaram, "Sensor selection for hypothesis testing: Complexity and greedy algorithms," in *2019 IEEE 58th Conference on Decision and Control (CDC)*. IEEE, 2019, pp. 7844–7849.

[30] Y. Lapshin, B. Blyuss, S. Dziuba, and L. Tatarko, "The choice of mining development strategy based on the improved bayes criterion," in *E3S Web of Conferences*, vol. 168. EDP Sciences, 2020, p. 00053.

[31] A. Borodin, M. Tvaronavičienė, I. Vygodchikova, G. Panaedova, and A. Kulikov, "Optimization of the structure of the investment portfolio of high-tech companies based on the minimax criterion," *Energies*, vol. 14, no. 15, p. 4647, 2021.

[32] C. Scott, "A generalized neyman-pearson criterion for optimal domain adaptation," in *Algorithmic Learning Theory*. PMLR, 2019, pp. 738–761.